NONLINEAR FINITE ELEMENT ANALYSIS OF PROFILED STEEL DECK COMPOSITE SLAB SYSTEM UNDER MONOTONIC LOADING

by

Shubhangi Attarde

Master of Civil Engineering, specialization in Structural Engineering,
Ryerson University, Toronto, ON, 2014

Bachelor of Civil Engineering,
Ryerson University, Toronto, ON, 2013

A project report

presented to Ryerson University

In partial fulfillment of the requirements for the degree of

Master of Engineering

in the Program of

Civil Engineering

Toronto, Ontario, Canada, 2014

AUTHOR'S DECLARATION

I hereby declare that I am the sole author of this thesis. This is true copy of the thesis, including any required final revisions, as accepted by my examiners.

I authorize Ryerson University to lend this thesis to other institution or individuals for the purpose of scholarly research.

I further authorize Ryerson University to reproduce this thesis by photocopying or by other means, in total or in part, at the request of other institutions or individuals for the purpose of scholarly research.

I understand that my thesis may be made electronically available to the public.

Author's Signature: _____ Date: _____

Nonlinear Finite Element Analysis of Profiled Steel Deck Composite Slab System under Monotonic Loading

Shubhangi Attarde, Master of Engineering, 2014

Department of Civil Engineering
Ryerson University, Toronto

ABSTRACT

This research concentrated on the nonlinear finite element (FE) modeling of one-way composite floor slab system comprising of profiled steel deck and two types of concrete namely, Engineered Cementitious Composites (ECC) and Self-Consolidating Concrete (SCC). Two FE models were developed based experimental results of composite slabs subjected to in-plane monotonic loading. The simulated load-deflection response, moment resistance, and shear bond capacity using two FE models were in reasonable good agreement with experimental results. The FE models were used in a comprehensive parametric study to investigate the effect of numerical model parameters such as mesh size, dilation angle, steel sheet-concrete interaction contact, material properties and composite slab span. In addition, FE models were used to determine shear bond parameters of ECC and SCC composite slabs that can be used for design purposes.

ACKNOWLEDGEMENTS

I would like to express my sincere gratitude to my research supervisor Dr. Khandaker M. A. Hossain without whom this study would not be accomplished. His persistent support, encouragement, and valuable suggestions have guided me throughout each stage of my graduate study. My knowledge on the specialized subject of my research study has enhanced significantly due to my supervisor's vast experience, and sophisticated understanding for which I am truly grateful.

And finally, I am deeply and forever indebted to my family, Mr. Bhaskar Attarde, Mrs. Pratibha Attarde, and Mr. Sunny Attarde for their love, encouragement, and support throughout my entire life.

TABLE OF CONTENTS

LIST OF TABLES

LIST OF FIGURES

LIST OF ABBREVIATIONS AND SYMBOLS

b	Slab width
L	Slab Span
t	Slab thickness
P	Total applied load
V_t	Support reaction
d_p	Effective slab depth
L_s	Shear span
L'	Distance in-between the slab supports
HPC	High performance concrete
ECC	Engineered cementitious composite
HPFRCC	High performance fiber reinforced cementitious composites
SCC	Self-consolidating concrete
FE	Finite element
CAE	Complete Abaqus environment

FEA	Finite element analysis
VMA	Viscosity modifying admixtures
PVA	Poly vinyl alcohol fiber
AAR	Alkali-aggregate reactivity
CDP	Concrete damage plasticity
d_t	Damage parameter in tension
$\bar{\varepsilon}_t^{ck}$	Cracking strain of concrete
ε_t	Total strain
σ_t	Tensile stress
E_o	Initial elastic stiffness of concrete
$\bar{\varepsilon}_t^{pl}$	Plastic strain in tension
σ_{c0}	Initial yield stress
σ_{cu}	Ultimate stress
d_c	Damage parameter in compression
$\tilde{\varepsilon}_c^{in}$	Inelastic or crushing strain
$\tilde{\varepsilon}_c^{pl}$	Plastic strain in compression
σ_{true}	True stress
ε_{ln}^{pl}	Logarithmic plastic strain
σ_{nom}	Nominal stress
ε_{nom}	Nominal strain
E	Modulus of elasticity
3D	Three-dimensional
C3D8R	Linear hexahedral solid element
S4R	Linear quadrilateral shell element

U1	Displacement in x direction
U2	Displacement in y direction
U3	Displacement in z direction
DOF	Degrees of freedom
ψ	Dilation angle in the p-q plane
ε	Flow potential eccentricity
σ_{b0}/σ_{c0}	Ratio of initial equibiaxial compressive yield stress to initial compressive yield stress
*K*c	Ratio of the second stress invariant on the tensile meridian
ES	Mesh element size
RP	Reference point
S11 or σ_{xx}	Principal stress in x direction
S22 or σ_{yy}	Principal stress in y direction
S33 or σ_{zz}	Principal stress in z direction
MPC	Multi-point constraints
f'_c	Compressive strength of concrete
m	Mechanical interlocking between concrete and profiled steel deck
k	Friction at the interface of concrete and steel deck
$\tau_{u,Rd}$	Shear bond capacity of slab
V_u	Ultimate shear capacity of slab
P_u	Two load in a four-point loading test
A_p	Cross-section area of profiled steel sheet

CHAPTER 1 – INTRODUCTION

1.1 General

Composite slab comprises of cold-formed profiled steel sheet and structural concrete toping is an optimum flooring system commonly used nowadays for the construction of buildings (Figure 1.1). Implementation of this structural system provides several advantages such as quick installation, reduced dimensions and weight of building floors, In addition, the steel deck serves as a permanent formwork for supporting the concrete (Gholamhoseini et al. 2014). The major benefit with using steel deck is that it acts as the external reinforcement for the slab to resist the tension induced by positive bending moment of the composite structure. To serve as tension reinforcement, it is crucial to achieve the transmission of horizontal shear stresses at the interface of concrete-steel surfaces, which is dominating factor that controls the composite action between the concrete and steel sheeting. As the tension behaviour is governed by the steel sheeting, the additional reinforcement shown in Figure 1.1 provides the positive bending resistance. The strength and performance of the composite slab is also influenced by other factors such as the profile, geometry and thickness of steel sheeting, concrete compressive strength, and span length of the slab (Gholamhoseini et al. 2014). By adopting suitable shape and detailing of the steel sheet profile, sufficient resistance against vertical separation and horizontal slippage can be achieved between the hardened concrete and steel deck.

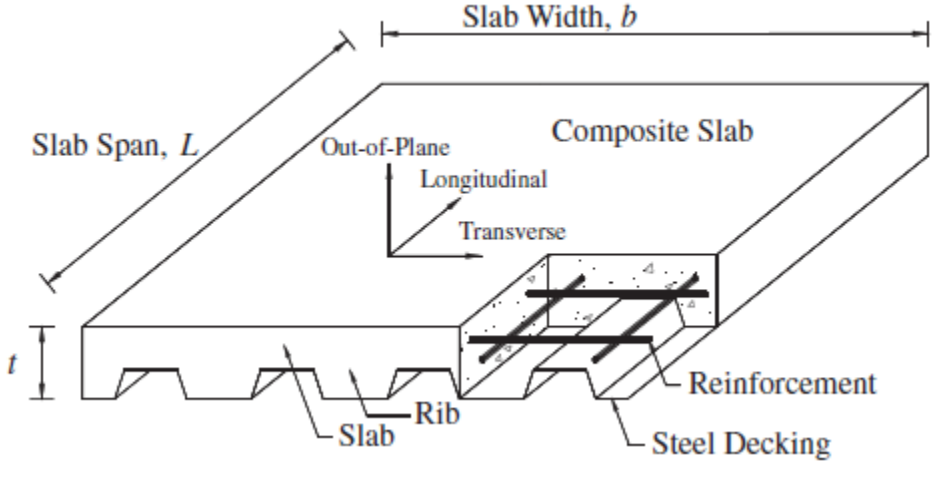

Figure 1.1: Components of a composite slab (Gholamhoseini et al. 2014)

A composite slab must be designed to sustain factored loads at the ultimate limit state. For this study, the performance of the composite slab was evaluated under a four-point bending test, for which there are

three major modes of failure: flexure failure at section b-b within peak moment region, vertical shear failure at section a-a, and horizontal shear failure at section c-c. Each of the mentioned sections correspond with the Figure 1.2, where, P is the total applied load on the composite slab, V_t is the support reaction at each support , b is the slab width, t is the slab thickness, d_p is the effective slab depth, L_s is the shear span and L' is the distance in-between the slab supports.

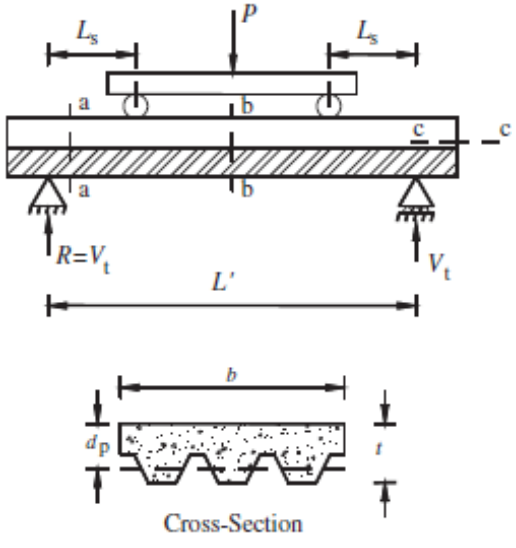

Figure 1.2: Failure modes of composite slab subjected to bending test (Gholamhoseini et al. 2014)

The flexural failure (mode b-b) requires absolute interaction between the concrete and steel sheeting surfaces, and this mode of failure usually dominates for long and thin slabs. However, as the composite slab length is generally restricted by the serviceability limit and with the lack of strong bond between the concrete and steel deck interface, this type of failure is not likely to threaten the performance of composite slab. For vertical shear failure to govern the slab must be very short and thick with a high magnitude of concentrated load positioned close to the supports, which does not resemble the setup of the four-point bending test that was imposed on the studied composite slab. The longitudinal shear failure is the most common type of failure to occur for majority of composite slab systems due to the shear failure at the interface of concrete-steel sheet. This type of failure is propagated with the development of a diagonal crack within the concentrated load region and significant end-slip between the concrete and steel sheeting, and steel sheeting, thus reducing the stiffness and strength of the composite steel deck floor slab.

According to Eurocode 4 (1994), “m-k” and “partial shear connection” are the two methods can be used for evaluating the longitudinal shear capacity of composite slabs. For this research the “m-k” method was

adopted to determine the shear bond characteristics of SCC and ECC composite slabs. The longitudinal shear capacity of the composite slab specimen is dependent on the geometry and flexibility of the selected type of steel sheeting, including the size and spacing of the steel deck embossments, and the span-to-depth ratio of the concrete slab (Gholamhoseini et al. 2014). The shear bond characteristics of the embossed profiled sheeting are defined with by two empirical constants m and k, which have the dimensions of stress. This method is applicable for composite slabs that exhibit both ductile and brittle longitudinal shear failure (Lam et al. 2008). In Eurocode 4 (1994), the defined criteria for ductile failure of composite slabs is that the failure load should exceed the load at the end slip of 0.1 mm by more than 10%, otherwise, it will be classified as brittle failure (Lam et al. 2008).

The low tensile strength of conventional concrete is the primary cause for the propagation of severe cracking in composite slabs. This leads to the development of steel reinforcement corrosion and significant increase in slab deflection. With decreasing budget allocations for infrastructure maintenance, rehabilitation, and replacement, there is a substantial need for the use new generation of high performance concrete (HPC) concrete for enhanced durability and structural performance.

1.2 Significance of the Research

Although structural performance of composite slabs with traditional concrete was the subject matter of numerous research studies, limited research has been conducted to envisage the behaviour of composite slabs with different profile steel sheeting and newly emerging high performance concrete (HPCs) (Mohammed et al. 2011; Mohammed, 2010; Hossain and Vinay, 2012). Structural behavior of composite slab using different concretes including rubber concrete have been investigated (Bashar 2010, Marimutu et al. 2007, Chen 2003, Makelainen and Sun 1999).

The better shear bond interaction between steel sheet and HPC can significantly improve the structural performance of composite slabs in addition to improve durability. Therefore the study of structural performance of composite slabs with different HPCs with varying profile geometry and mechanical connectors is warranted. Design of composite slabs can be achieved by using m-k method, if m (parameter that defines shear bond due to mechanical interlock between steel and concrete) and k (parameter that defines shear bond due to friction between steel and concrete) values are known from experiments. M and k values normally change with different concrete and different steel sheets (Mohammed 2010; Eurocode 4 1994). Composite slabs with better structural performance can be obtained by using newly

developed high performance concretes (HPCs) especially emerging highly ductile Engineered Cementitious Composite (ECC).

Engineered Cementitious Composite (ECC) is a new generation of high performance fiber reinforced cementitious composites (HPFRCC). The primary function of ECC is to provide high tensile ductility and strain capacity while maintaining self-controlled tight micro-crack widths (Sahmaran et al. 2007, and Li et al. 2011, Afefy and Mahmoud 2014).

Cost-effective highly flowable green ECCs (developed recently at Ryerson University) made of locally available materials (Hossain 2014; Hossain and Anwar 2014; Sherir et al. 2014) could yield better composite action between the profiled steel sheeting and the concrete. The high strain capacity (300 to 500 times greater than normal concrete) while maintaining low crack widths (less than 60μm) could resolve the problems through shear bond optimization and improving constructability (faster construction and better concrete quality control through self-consolidation) as well as enhancing ductility and durability (Hossain and Vinay, 2012). Use of ECC for composite slabs can achieve compatible properties, such as compressive strength, thermal expansion, in addition to providing resistance against large tensile and shear forces (Hossain and Vinay, 2012).

No research has been conducted on the development of high performance composite slabs using ECC. There is an urgent need to conduct research on the structural performance of ECC based composite slabs compared to their traditional concrete counterparts and develop design specifications. Past research studies conducted on nonlinear finite element (FE) modeling of composite slabs were mainly focused on using conventional concrete material. It is also crucial to develop nonlinear FE models of composite slabs made of ECC and SCC.

1.3 Scope and Objective

The main objectives of this study are to:

- develop nonlinear finite element (FE) models of SCC and ECC composite slab using ABAQUS/CAE based on experimental data and validate the performance of models
- perform comprehensive parametric studies to investigate the effect of ABAQUS modeling parameters (mesh size, types of interface contact, simulation type -load/displacement control etc.), concrete/steel sheet material properties and variable composite slab span length on load-displacement response, stiffness, failure loads and stress characteristics of ECC and SCC composite slabs.

- Use developed FE models to simulate the behavior of numerical ECC/SCC composite slabs having variable total and shear span to evaluate ultimate load/moment resistance and the shear bond characteristics. Compare experimental and FE predicted ultimate load/moment resistance and the shear bond to verify the accuracy of the proposed FE models.
- Suggest design aids in the form tables for the prediction of load/moment resistance and steel-concrete shear bond of ECC and SCC composite slabs for variable span length.

1.4 Outline of Report

This report consists of 7 chapters which can be outlined as follows:

Chapter 1 presents a brief introduction about the composite slabs, the significance of this research followed by the objectives of this study.

Chapter 2 presents a literature review on the development of steel deck composite slabs and finite element modeling methods based on previous research studies.

Chapter 3 provides a brief description of the experimental program and the material properties. It also presents the experimental test results for monotonic loading in the format of load versus displacement for SCC and ECC composite slabs that were used to develop and validate FE models results.

Chapter 4 presents a detailed description of the finite element models developed to simulate the behaviour of SCC and ECC composite slabs under monotonic loading condition. Some strategies in nonlinear dynamic explicit FE method for simulating a quasi-static response are also briefly discussed.

Chapter 5 explains the deficiency with using the load control analysis for ABAQUS/CAE nonlinear FE modeling. The outputs obtained from load control analysis are presented to verify this hypothesis. Moreover, the parametric study is conducted for load control analysis investigating the influence of dilation angle and mesh sensitivity.

Chapter 6 presents the FE models based on the displacement control analysis for ECC/SCC composite slabs. The load-deformation response from the Finite Element Analysis (FEA) and experimental results are also compared for both SCC and ECC composite slabs to evaluate the prediction accuracy of the two models. It also presents the results of parametric study to study the influence of ABAQUS modeling parameters. Developed FE models are used to determine load/moment resistance and shear bond capacity of numerical ECC/SCC composite slabs to produce design aids.

Chapter 7 presents the main conclusions and recommendations for future research studies.

CHAPTER 2 – LITERATURE REVIEW

2.1 Introduction

Composite floor is a structural system that uses the composite action between the steel deck and the concrete. In this chapter, the development and recent investigations on different types of innovative composite slab systems are presented, In addition, a brief overview of research on the finite element analysis simulating the behaviour of composite slabs is also presented.

2.2 Development of Composite Steel-Deck Concrete Floor System

Many researchers studied the behaviour and design of steel deck composite slabs since the late 1960s. Ekberg and Schuster (1968), and Schuster (1976) introduced the construction industry to the different composite floor systems, such as the concrete slabs that utilize transverse wires, embossments on flanges and webs of the steel sheeting. In conjunction with these studies, Porter and Ekberg (1976) provided the design recommendations for the profiled composite floor slabs. Their research led to the formation of the basis for the ASCE (1984) standard procedures for designing composite slabs and established the linear regression methods for meeting the testing requirements.

Wright et al. (1987) emphasized on the structural, construction, and economical advantages of implementing profiled steel sheeting in the production of composite floor systems. The research included over 200 tests on the elements of composite steel deck slab, and the results were validated with the design methods to study the aspects of construction phase, composite slab and steel beam action phase. Makelainen and Sun (1999) studied the longitudinal shear resistance of a new steel sheeting profile for composite floor slabs, which revealed that as the depth of the embossments increased, rather than the length or the shape, it had proportionally increased the magnitude of shear stresses as well, thus providing better resistance against separation of steel deck and profiled concrete. In-plane shear resistance of the profiled steel deck, profiled concrete panels and the double skin-profiled composite shear panels were investigated (Hossain 1995, Hossain and Wright 1998, 2004a, b).

Marimutu et al. (2007) conducted an experimental investigation to study the shear bond behaviour of the embossed composite deck slab under simulated imposed loads using conventional concrete. For this research, six set of slabs were tested, each comprised of three slabs with altered shear span for each set. For testing shorter shear loading, the shear span of 320 mm, 350 mm, and 380 mm were used; and for

longer shear loading the shear span of 850 mm, 950 mm, and 1150 mm were selected. Based on this test results it was determined that the behaviour of the composite slab depends on the shear span length. Failure of the shorter shear span slab was governed by shear bond failure, whereas, for longer shear spans the slab responded with flexural failure.

For studying the influence of advanced concrete properties, Bashar (2010) examined the structural response of the composite concrete slab consisting of crump rubber concrete. This experimental test included two set of slabs with shear span of 450 mm and 900 mm, respectively. Each set comprised of four slabs in total, of which three slabs were composed of rubbercrete and one slab was made with conventional concrete as control slab. The test results verified the ductile response of the rubbercrete slabs. For analyzing the influence of different end restraints on shear-bond action of simply supported composite slabs, Chen (2003) tested seven simply supported one-span composite slabs and two continuous composite slabs. The experimental results revealed that the slabs with end anchorage of steel shear connectors had higher shear-bond strength capacity in comparison to the slabs without end anchorage.

2.3 Review of FE Methods Applicable to Composite Slabs

For composite slabs, various models have been proposed to perform the finite element (FE) analysis. Daniels and Crisinel (1993a, b) developed a FE method using the plane beam elements to evaluate the performance of single and continuous span composite slabs. The procedure accounts for the nonlinear behaviour of materials such as concrete, and the shear interaction property between the concrete and steel sheeting surfaces was defined based on the results obtained from the pull out test that was conducted by the authors. Veljkovic (1996) performed three-dimensional finite element analysis using the software DIANA to analyze the behaviour of the concrete-steel sheet interface in the composite slab. The shear interaction between the concrete and steel sheet was modeled by using the nodal interface element and its property was defined based on the results from the push tests. Abdullah and Easterling (2007) developed a design procedure that can use bending test results to produce a suitable shear bond property for a given specimen of steel deck composite slab. The generated shear-bond slip curves were used in FE models to define the properties of the connector elements and simulate the horizontal shear bond behaviour in composite slabs. The FE analysis model generated by Widjaja (1997) used two parallel Euler-Bernoulli beam elements to simulate the bending test response of composite slab. The key difference between the model generated by Widjaja and the others was that only one single longitudinal section of

the composite slab model was used, and the vertical node displacements of the two elements were restricted to be equivalent in magnitude and direction.

The main shortcoming of these proposed FE procedures is that the interface contact property between the concrete and profiled steel sheeting was predefined. Moreover, it is unlikely to achieve the equivalent shear bond interface response with push-out and bending tests. The shear bond interaction in the composite slabs between the concrete and the profile steel deck is difficult to model due to its nonlinear contact which must account for concrete stickiness, allow for concrete sliding against steel sheeting, and simultaneously use the friction phenomena between the two components to minimize and slow down the sliding motion at the interface (Chen et al. 2011). Ferrer et al. (2006) performed the pull-out tests on composite slabs using the FE method, in which the interface contact elements were established between the concrete and steel sheeting and the behaviour of the slab specimen were analyzed for various friction coefficients. However, the deficiency with this method was that the failure was not executed with the rigid concrete surface.

Input via a text-based file and graphical interactive method are the two methods that can be used in ABAQUS (CAE) to conduct the finite element analysis. The text file format is suitable approach for modeling two-dimensional FE models, however, the procedure becomes complex for performing three-dimensional nonlinear finite element modeling and analysis of composite slabs. Abdullah (2004) developed a finite element model for composite slabs with ABAQUS/Explicit 6.3 using the text-based file format. The interaction between the concrete and the steel deck was modeled with radial-thrust type connector elements (CONN3D2), as shown in Figure 2.1.

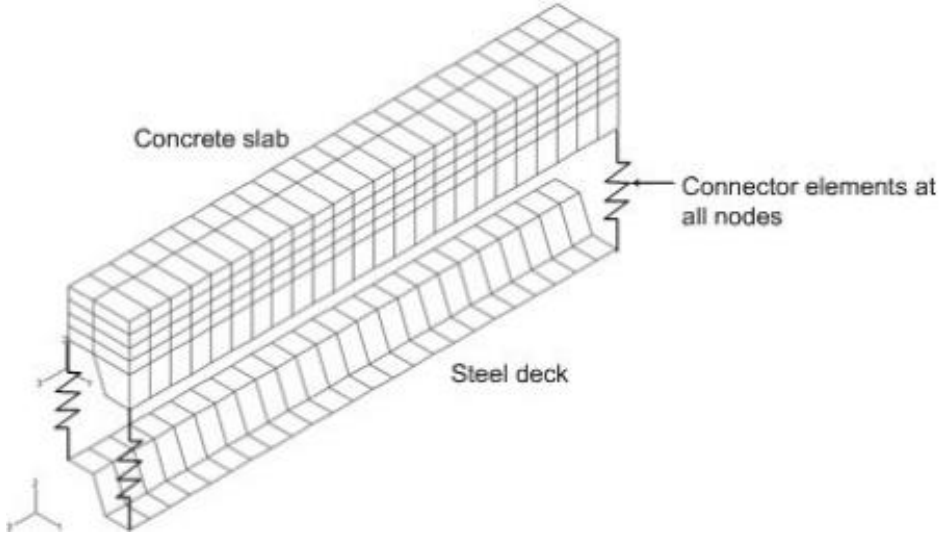

Figure 2.1: FE model of composite slab using connector elements (Abdullah 2004)

The connector was established between the concrete and steel nodes that are closest to each other. With Abdullah (2004) model, the vertical interaction and the frictional resistance of the support was not considered due to the assumption that its effect was implicitly present in the horizontal shear property. This model is feasible for small scale specimen testing, however, for large-scale composite slab models using graphical interaction modeling is recommended.

2.4 Self-Consolidating Concrete (SCC)

Self-Consolidating Concrete (SCC), one of the latest innovations in high-performance concrete, is a highly flowable concrete that can easily spread into a structural formwork under its own weight. Good consolidation can be achieved with SCC, eliminating the need for external or internal vibrators and yet exhibiting homogeneous mix without segregation or excessive bleeding. Self-consolidating concrete can be used to facilitate concrete placement and the productivity of casting congested and narrow structural members such as slabs (Khayat 1999).

Self-consolidating concrete was developed in Japan during the early 1980's (Hayakawa et al. 1993). In addition to fulfilling the demand of a flowable concrete that can properly consolidate the heavily reinforced seismic members, it was also developed to improve the on-site working conditions such as reducing time and cost of construction, requiring less labour workers, and eliminating the noise and pollution caused due to vibrators.

There are several different methods that can be used for producing self-consolidating concrete mix. One approach could be to substantially increase the fine material content such as fly ash and slag cement, while maintaining constant amount of water. A research study conducted by Bouzoubaâ and Lachemi (2001) has proved that using high volume of Class F fly ash can also result in an economical mix design of SCC.

An alternative design approach would be to utilize viscosity modifying admixture (VMA) to develop the stability of the SCC mix. According to the study performed by Lachemi et al. (2003), the behaviour of twenty-one concrete mixtures were tested with three types of manufactured SCC consisting of fly ash, slag cement, and three different VMAs. Based on the test results, it was learnt that the selected three materials were able to successfully develop an economical SCC with desired properties; and VMA was capable of providing higher resistance to segregation and early strength development in comparison to fly ash and slag cement.

2.5 Engineered Cementitious Composites (ECC)

Engineered Cementitious Composites (ECC), a category of ultra-ductile fiber reinforced cementitious composites, was originally invented at the University of Michigan during the early 1990s (Li 1993). ECC is characterized by high ductility in the range of 3-7%, tight self-controlled crack width of maximum 60 µm, and with low fiber volume typically close to 2% (Sahmaran et al. 2009a and Zhou et al. 2010). The most common type of fiber used in engineered cementitious composites is poly vinyl alcohol (PVA) fiber with a diameter of 38 µm and length of approximately 12 mm (Li 1993).

The main advantage of using ECC is its ability to develop pseudo strain-hardening after the first crack with a composite strain capacity that is 300 to 500 times higher than conventional concrete, similar to the response of a ductile metal (Sahmaran et al. 2009a). As shown in Figure 2.2, the crack width of ECC remains less than 60 µm while sustaining large imposed deformations.

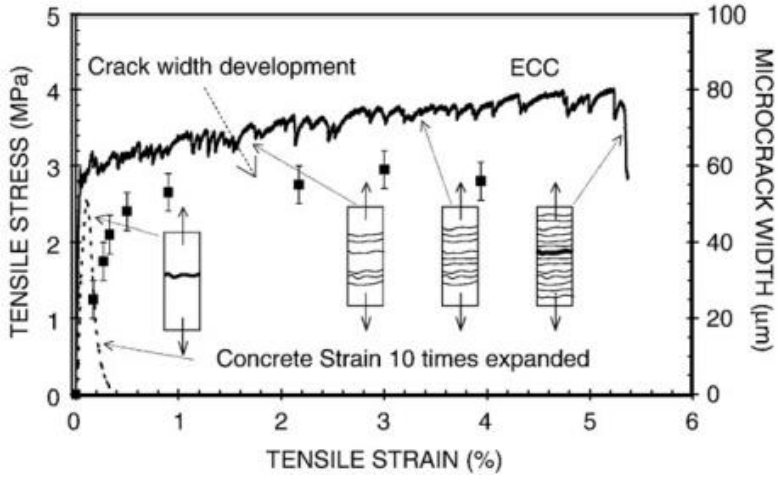

Figure 2.2: Tensile stress-strain curve and tight crack width control of ECC (Sahmaran et al. 2009a)

The reason for the high ductility and strain capacity of ECC is due to the optimization of its material properties through the application of micromechanics (Li 1993, Sahmaran et al. 2009b). Micromechanics quantify the influence of a material structure on macroscopic behaviour by accounting for bridging interaction among the fiber, the mortar matrix and fiber-mortar interface matrix. Matrix heterogeneities in ECC include the cement grain, sand particles, and mineral admixture particles, with the particle size ranging from nanometer to millimeter scale (Nawy 2008).

2.6 Review Conclusion

The provided literature review demonstrates that the analysis of the profiled steel-deck composite slab behaviour is intricate. Majority of the experimental tests were performed with the conventional concrete. Little research has been conducted to date on the structural performance of composite slabs with Engineered Cementitious Composite (ECC). Moreover, FE analysis of ECC based composite slab has not yet been performed. This research focusing on finite element (FE) simulation of the profiled composite slab utilizing the ECC and SCC is a timely initiative and will contribute to the advancement of the knowledge.

CHAPTER 3 – EXPERIMENTAL PROGRAM

3.1 Introduction

For this study, experimental data from the research conducted at the Ryerson University by Hossain et al. (2014) was used. A total of twelve composite slab specimens were tested with two types of profiled steel sheets (designated as P3623 and P2432) and two types of concrete (ECC and SCC). SCC and ECC composite slabs prepared with P-3623 steel deck (as shown in Figure 3.1a) was selected to perform the nonlinear FE modeling. The dimensions of ECC and SCC composite slabs are 1800 mm (length) x 960 mm (width) x 100 mm (depth). Of the total slab depth, 49 mm is the depth of the concrete and 51 mm is the height of the steel deck. The supports for the composite slabs were located 150 mm away from the span ends, and the monotonic loading was applied in the form of four-point bending test. Figures 3.1(a-b) provide detail dimensions of the chosen composite P-3623 steel deck slabs chosen for FE modelling.

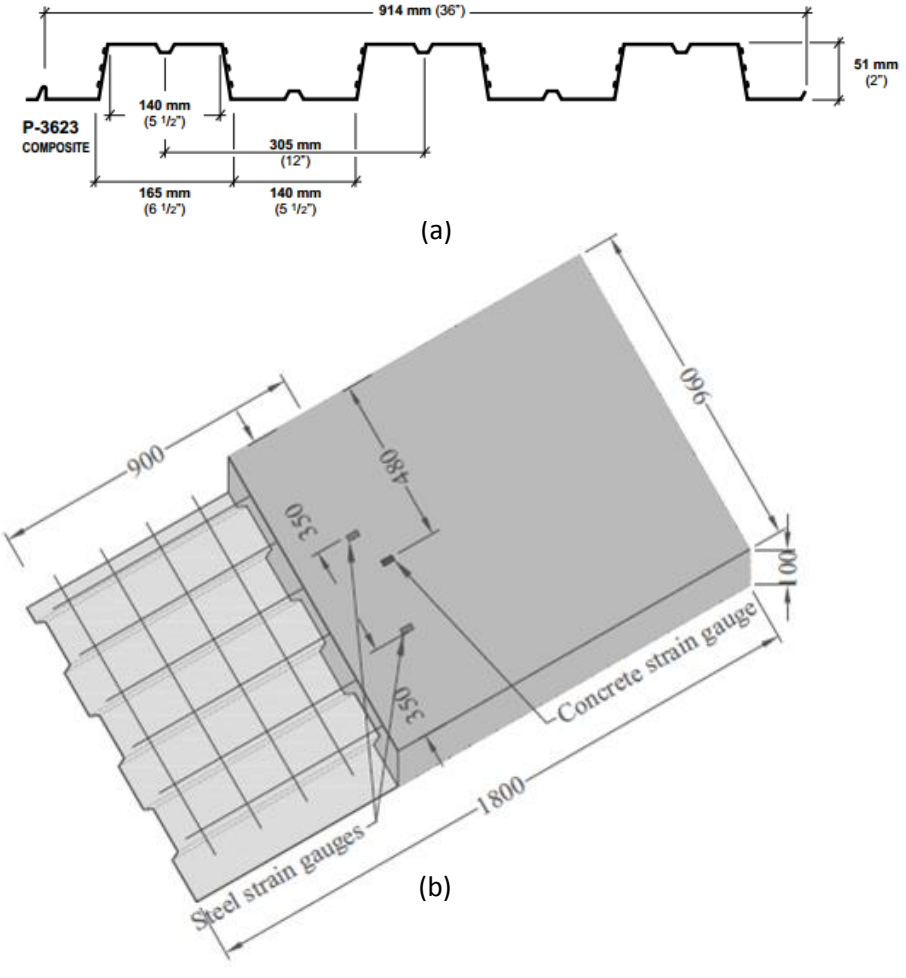

Figure 3.1: (a) Dimensions of P-3623 steel deck (Canam Group 2006), (b) 3D model of composite-3623 steel deck slab (Hossain et al. 2014)

3.2 Material Properties

In reference to Hossain et al. (2014), two concrete mixtures were used for the composite slabs – a Ryerson produced green Engineered Cementitious Composite (ECC) and a commercial Self-Consolidating Concrete (SCC) produced by King Packaged Materials. ECC was composed of PVA fibers (8 mm length and diameter of 39µm diameter), local mortar sand (instead of silica sand), Portland cement, fly ash (as 55% replacement of cement content), admixtures and water-to-binder ratio of 0.27. KING SCC is a pre-blended, pre-packaged, high performance, flowable concrete material containing Portland cement, silica fume, 10 mm stone and other selective admixtures (KING MS-S10 SCC, 2014). KING SCC is designed with natural normal-density non-reactive fine and coarse aggregates to eliminate the potential of generating alkali-aggregate reactivity (AAR). The strength properties of the selected ECC and commercial SCC, determined from control specimens at the age of testing (at 28 days) of composite slabs, as per ASTM Standards (ASTM C39 2012; ASTM C78 / C78M 2010) are presented in Table 3.1.

Table 3.1: Concrete strength properties

Specimen	Cylinder Concrete strength (f'_c) (MPa)	Flexural strength (MPa)
P3623-ECC	66	6.2
P3623-SCC	56	4.8

3.3 Test Results: Load-deflection Behaviour

According to Hossain et al. (2014), Figure 3.2 presents the load-deflection responses of six of the total twelve composite slabs selected for FE modeling. Figure 3.2a and 3.2b, each presents three load-deflection curves for ECC and SCC composite slab with Canam composite P-3623 steel deck, respectively. ECC and SCC composite slabs were loaded to failure at three different shear span distances - 300 mm, 450 mm, and 600 mm. These experimental curves were used to develop FE models presented in Chapter 6. The accuracy and performance of FE models were tested by comparing FE based load-deflection responses with those obtained from experiments.

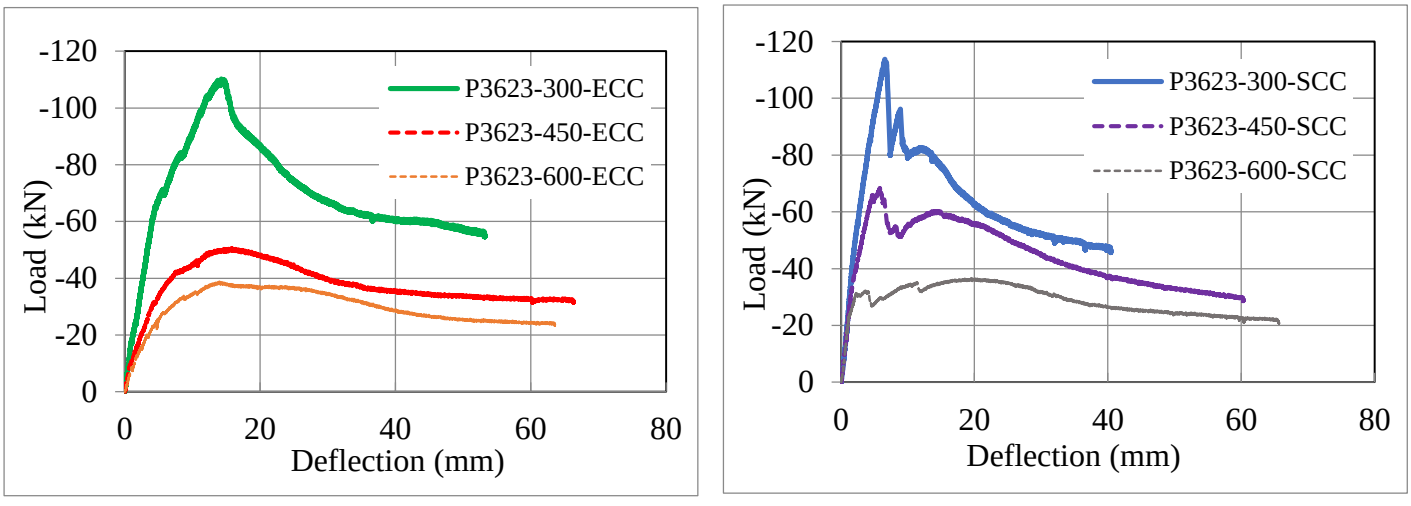

(a) (b)

Figure 3.2: Load-deflection response of composite specimens with variable shear spans (a) P3623-ECC and (b) P3623-SCC (Hossain et al. 2014)

3.4 Summary

In this chapter, the experimental load-deflection results for six composite slab specimens tested under monotonic loading are presented. Summary of the key experimental results used to validate the nonlinear finite element models of ECC and SCC composite slabs are presented in Table 3.2.

Table 3.2: Summary of experimental results for monotonic loading

Type of Composite Slab	Shear Span (mm)	300	450	600
P3623-ECC	Ultimate Load (kN)	110.20	50.54	38.77
	Mid-span Displacement (mm)	14.27	15.83	14.00
P3623-SCC	Ultimate Load (kN)	113.75	68.43	36.66
	Mid-span Displacement (mm)	6.58	5.82	3.51

CHAPTER 4 – FINITE ELEMENT MODELING OF COMPOSITE SLAB SUBJECTED TO MONOTONIC LOADING

4.1 Introduction

Finite element (FE) analysis of composite slab was executed to develop models based on the experimental results. The primary objective was to develop reliable three-dimensional finite element (FE) model which can simulate the behaviour of ECC and SCC composite slabs subjected to monotonic loading. In this research, the model was developed using ABAQUS/CAE (Dassault Systèmes Simulia Corp. 2013).

4.2 General Overview of ABAQUS/CAE

ABAQUS/CAE provides a collaborative graphical environment that allows for simple modeling and generating complex geometry into optimized mesh regions. Material properties, loads, and boundary conditions can be discretely assigned to the geometry. ABAQUS/Standard and ABAQUS/Explicit are the two main types of analysis products in this software. Of which, ABAQUS/Standard is used for general-purpose analysis that solves a system of equations implicitly at each result increment. It is capable of resolving an inclusive range of linear and nonlinear problems including static, dynamic, thermal, and electrical response of elements. ABAQUS/Explicit is a distinct-user analysis module that uses an explicit dynamic integration without the requirement of having equations of motion solved at each time increment. Table 4.1 provides a brief comparison between ABAQUS/Standard and ABAQUS/Explicit which was excerpted from the ABAQUS manual (Dassault Systèmes Simulia Corp. 2013).

Table 4.1: Major differences between ABAQUS/Standard and ABAQUS/Explicit (Dassault Systèmes Simulia Corp. 2013)

Parameter	**ABAQUS/Standard**	**ABAQUS/Explicit**
Element Library	Offers an extensive element library	Offers an extensive library of elements well suited for explicit analyses. The element available in ABAQUS/Standard
Analysis procedures	General and linear perturbation procedures are available	General procedures are available
Material models	Offers a wide range of material models	Similar to those available in ABAQUS/Standard; a notable difference is that failure material models are allowed

Contact formulation	Has a robust capability for solving contact problems	Has a robust contact functionality that readily solves even the most complex contact simulations
Solution technique	Uses a stiffness-based solution technique that is unconditionally stable	Uses an explicit integration solution technique that is conditionally stable
Disk space and memory	Due to the large numbers of interactions possible in an increment, disk space and memory usage can be large	Disk space and memory usage is typically much smaller than that for ABAQUS/Standard

The Finite Element Analysis (FEA) for this study was conducted using ABAQUS/Explicit mainly to enhance the following performance aspects:

- To avoid the convergence difficulties in ABAQUS/Standard (implicit) program which progressively develops due to the concrete degradation
- Using ABAQUS/Explicit reduces the computational time for the three-dimensional composite slab model
- It is efficient in modeling non-linear dynamic events with contact interaction and discontinuous geometrical or material responses.

4.2.1 Quasi-Static Analysis with ABAQUS/Explicit

The explicit solution is a true dynamic process that was originally established to model high-speed impact events with inertia serving as a main criterion in the solution. When applying quasi-static simulations using explicit dynamics, it is computationally impractical to analyze the model in its natural time scale. As it would require the use of large number of small time increments, the most feasible solution can be obtained by accelerating the analysis time. In this study, the following two techniques were used to simulate the quasi-static condition in the monotonic loading:

1.) Smooth amplitude curves: To achieve highly accurate and efficient results in quasi-static analyses the gradual application of displacement produces a smooth change in slope of velocity and acceleration. Instantaneous loading can cause the buildup of stress waves throughout the model, which can produce noisy or inaccurate solutions, as demonstrated in the parametric study comparison in Chapter 6. To apply the displacement in the smoothest possible manner requires the change in displacement to remain as a small amount in-between two increments. This is automatically achieved in ABAQUS/CAE with the built-in smooth step amplitude curve that efficiently commends the displacement in a quasi-static condition.

2.) Loading rates: The time step used in the developed composite slab FE models was one second. It is practical to assume that performing an analysis within the duration of actual time required for a quasi-static process will produce accurate static results. As illustrated in Chapter 6, a series of analyses at varying displacement and load rates was performed to determine a reasonable displacement rate.

4.3 Material Properties

4.3.1 Concrete Model

ABAQUS/CAE Version 6.13-3 consists of three different models to simulate the concrete behaviour; the smeared cracking model, brittle cracking model, and the concrete damaged plasticity model (Dassault Systèmes Simulia Corp. 2013). Each of these model types have their application limitations and can serve effectively for only certain types of structures and loading conditions.

4.3.1.1 Concrete Damage Plasticity

The Concrete Damage Plasticity (CDP) (Lubliner et al. 1989, and Lee et al. 1998) is the most comprehensive continuum model that was used in the composite slab simulation to define concrete behaviour in this analysis. The CDP model is applicable to concrete that is subjected to monotonic loading for different types of structures (such as beams, trusses, shells, and solids) and it is developed based on two concrete failure mechanisms: compressive crushing and tensile cracking. For this study, the model had used isotropic damaged elasticity in correlation with isotropic compressive and tensile plasticity to characterize the inelastic nature of the concrete. Modeling more than one interaction with concrete can be difficult in ABAQUS/CAE. Thus for the simplicity of FE model analysis, the effect of including reinforcement was taken into consideration by introducing some “tension stiffening” into the composite slab modeling to simulate the load transfer across cracks through the rebar. The rebars in the composite slab mainly serve as positive reinforcement because the profiled steel sheet is the main element that provides tensile resistance. The response of concrete in compression and tension was modeled based on the guidelines described in the ABAQUS user manual (Dassault Systèmes Simulia Corp. 2013).

4.3.1.2 Concrete Behaviour in Tension and Compression

For concrete subjected to uniaxial loading, the stress-strain response of concrete in tension exhibits a linear elastic relationship until the failure stress is achieved and beyond that point the concrete follows the softening stress-strain behaviour. When the concrete is unloaded at any point from within the strain-softening portion of the curve, the unloading response is weakened and the elastic stiffness of concrete is damaged. This deterioration of the stiffness is defined by damage parameter in tension (d_t), which can range from zero, representing the undamaged condition of the specimen, to one, which signifies that the material has lost its total strength. Figure 4.1 illustrates the concrete behaviour in tension, when subjected to uniaxial loading.

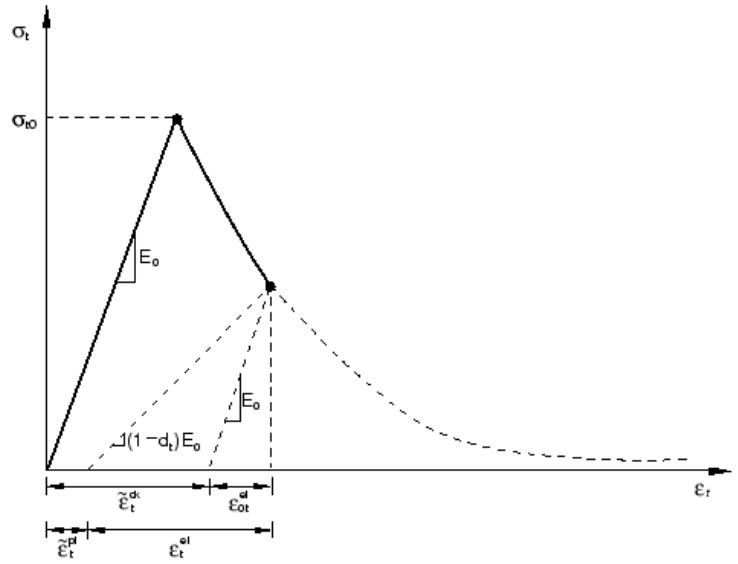

Figure 4.1: Stress-strain response of concrete in tension subjected to uniaxial loading in ABAQUS (Dassault Systèmes Simulia Corp. 2013)

The cracking strain ($\bar{\varepsilon}_t^{ck}$) is calculated by ABAQUS as the difference between the total strain (ε_t) and the elastic strain that corresponds to the undamaged material; given as Eq. 4.1:

$$\bar{\varepsilon}_t^{ck} = \varepsilon_t - \sigma_t / E_o \tag{4.1}$$

In this equation, σ_t is the tensile stress and E_o is the initial elastic stiffness of concrete. Tension stiffening data values are provided in terms of the cracking strain, $\bar{\varepsilon}_t^{ck}$. The unloading data are inputted in ABAQUS with tension damage curves (d_t versus $\bar{\varepsilon}_t^{ck}$). ABAQUS/CAE automatically converts the cracking strain data to plastic strain ($\bar{\varepsilon}_t^{pl}$) using the following Eq. 4.2:

$$\bar{\varepsilon}_t^{pl} = \bar{\varepsilon}_t^{ck} - \frac{d_t}{(1-d_t)}\frac{\sigma_t}{E_o} \quad (4.2)$$

Figure 4.2 draws a comparison between the defined tensile behaviour of SCC and ECC concrete damage plasticity model. As illustrated, the maximum yield stress for ECC is 6.2 MPa, while SCC has a yield stress capacity of 4.8 MPa. The key difference is the cracking strain of these two types of high-performance concretes. SCC tensile cracking strain represents strain factor of 1.0, based on which, the ECC tensile cracking strain values was determined as strain increment factor 2.0 to achieve the desired nonlinear FE load-deflection response, while simulating behaviour that accounts for ECC post-stiffening due to fibers. After conducting the parametric study, as presented in Chapter 6, on the effect of strain increment factor on the ECC composite slab behaviour, it was observed that the using strain multiplication factor of 2.0 provided the most feasible ECC concrete response that reasonably correlated with the experimental results.

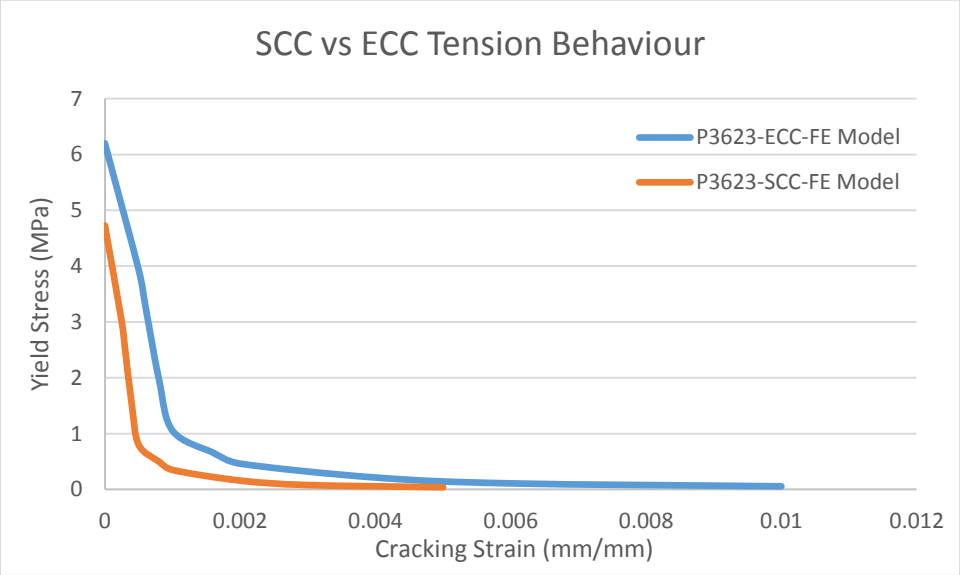

Figure 4.2: P3623-ECC and P3623-SCC concrete tension response

Under uniaxial loading, the concrete response in compression is linear until the initial yield stress (σ_{c0}) value is reached. In the plastic region, the characterization of concrete behaviour is typically initiated with stress hardening and then followed by strain softening beyond the ultimate stress (σ_{cu}) value. Similar to concrete behaviour in tension, the weakened elastic stiffness of concrete in compression is characterized with damage parameter (dc) for the equivalent scale ranging from zero to one. Figure 4.3 illustrates the concrete behaviour in compression when it is subjected to uniaxial loading.

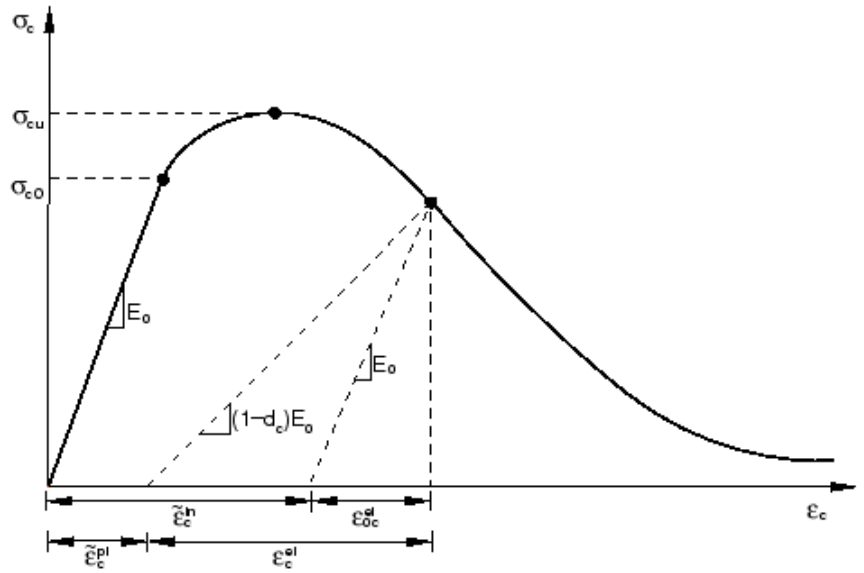

Figure 4.3: Compression stress-strain response of concrete subjected to uniaxial loading in ABAQUS (Dassault Systèmes Simulia Corp. 2013).

Compressive yield stress values are provided in ABAQUS as a tabular function of inelastic or crushing strain($\tilde{\varepsilon}_c^{in}$). The input of compressive stress and strain values are required to be positive (absolute) values. The compressive hardening data are provided in terms of inelastic strain($\tilde{\varepsilon}_c^{in}$), rather than plastic strain ($\tilde{\varepsilon}_c^{pl}$), which is determined as the difference between the total strain and the elastic strain that corresponds to undamaged material as provided in Eq. 4.3:

$$\tilde{\varepsilon}_c^{in} = \varepsilon_c - {}^{\sigma_c}/_{E_o} \tag{4.3}$$

In this equation, E_o represents the elastic stiffness of concrete. The unloading concrete information is provided to ABAQUS in the form of compressive damage curves ($d_c$versus $\tilde{\varepsilon}_c^{in}$). Similar to the tension behaviour, ABAQUS also automatically converts the inelastic strain into plastic strain ($\tilde{\varepsilon}_c^{pl}$) using the following Eq. 4.4:

$$\tilde{\varepsilon}_c^{pl} = \tilde{\varepsilon}_c^{in} - \frac{d_c}{(1-d_c)}\frac{\sigma_c}{E_o} \tag{4.4}$$

The stress-strain curve past the ultimate stress value is defined as strain-softening regime, due to which ABAQUS cannot model ECC, as it requires the strain hardening to progressively develop as the ultimate stress value is reached. Thus, to obtain this anticipated ECC post-failure response it is vital to modify the "Concrete Damage Plasticity" model subroutine in ABAQUS, which can be the subject matter of future research on nonlinear finite element modeling of ECC composite slab.

Figure 4.4 illustrates two different compression responses that were used to define the "Concrete Damage Plasticity" model for ECC and SCC finite element model. ECC composite slab demonstrates superior compression response due its higher compressive strength capacity of 66 MPa in comparison to SCC with a strength of 56 MPa. As observed, the inelastic strain values for ECC in compression is taken as strain increment of 1.1 in comparison to SCC because significant increase in the compressive strain did not produce reasonable variability in finite element results for ECC composite slab. Moreover, as 56 MPa is relatively high compressive strength for SCC, therefore the compression response was also enhanced.

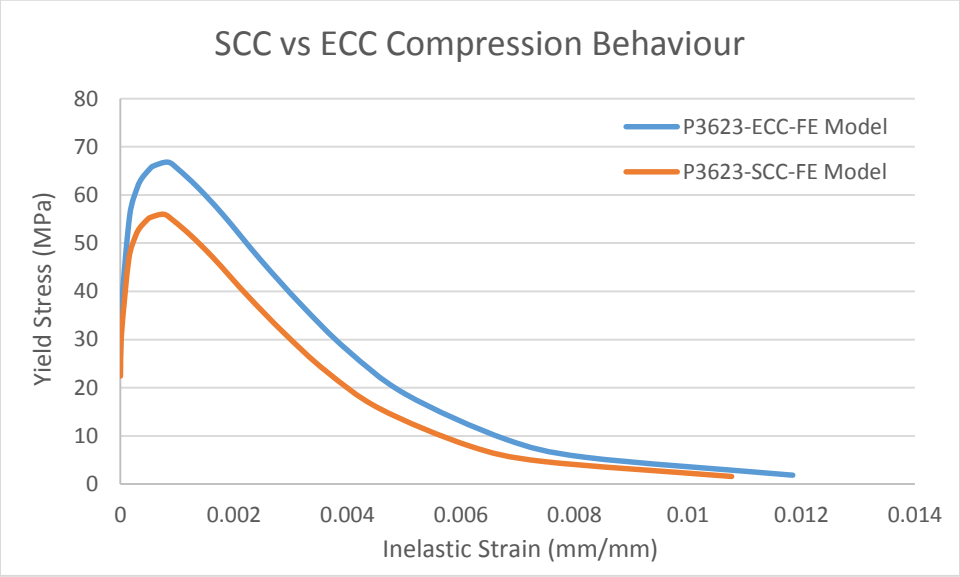

Figure 4.4: P3623-ECC and P3623-SCC concrete compression response

4.3.2 Steel Model

ABAQUS/CAE uses true (Cauchy) stress and logarithmic strain to perform the finite element analysis of steel, which can be derived from the tensile coupon test results. The following two equations, Eq. 4.5 and Eq. 4.6, derived by Lubliner (1990) were used in this research study to determine the true stress (σ_{true}) and logarithmic plastic strain(ε_{ln}^{pl}):

$$\sigma_{true} = \sigma_{nom}(1 + \varepsilon_{nom}) \tag{4.5}$$

$$\varepsilon_{ln}^{pl} = \ln(1 + \varepsilon_{nom}) - \frac{\sigma_{true}}{E} \tag{4.6}$$

In the provided equations, σ_{nom} represents the nominal stress, ε_{nom} is the nominal strain, and E represents the modulus of elasticity. Figure 4.5 illustrates the plastic behaviour of the composite P-3623 steel deck that was used in ABAQUS to define the yield stress and plastic strain tabular data.

For specifying the initiation of plastic flow in the state of multi axial stress in ABAQUS/Explicit, the Von-Mises yield surface criterion was utilized. For monotonic loading in ABAQUS, isotropic hardening model was specified, which generated a yield surface that exhibited uniform changes in size with respect to each direction such that the yield stress increases (or decreases) as the plastic strain develops in all stress directions (Davis and Selvadurai 2002).

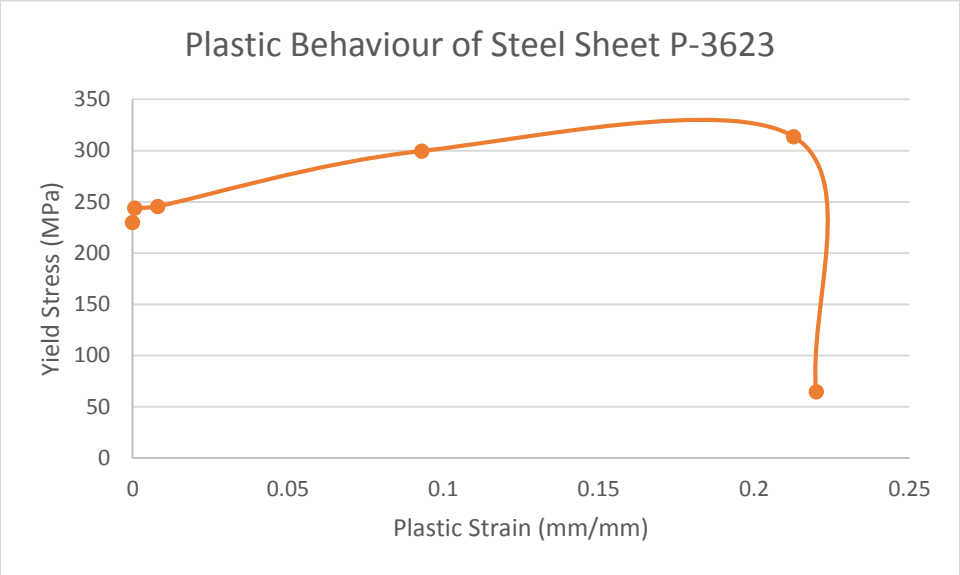

Figure 4.5: Canam composite P-3623 steel deck plastic response

For ABAQUS FE model, the provided Table 4.2 presents defined material properties for the two parts of the FE model, which are the profiled concrete and steel deck.

Table 4.2: ABAQUS concrete and steel material characterization

Property	**Value**
Part 1 : Concrete	Modeling Space: 3D Type: Deformable Shape: Solid, Homogenous Type: Extrusion Approximate size: 1000
Part 2: Steel Sheeting	Modeling Space: 3D Type: Deformable Shape: Shell, Homogenous Type: Extrusion Approximate size: 1000

Concrete Properties	**Value**
Density	2400 kg/m^3
Young's Modulus	30 GPa $(3 \times 10^{10}\ Pa)$
Poisson's Ratio	0.2
Steel Sheeting Properties	**Value**
Density	7000 kg/m^3
Young's Modulus	230 GPa $(2.30 \times 10^{11}\ Pa)$
Yield Stress	230 MPa $(2.30 \times 10^{8}\ Pa)$
Poisson's Ratio	0.30
Plastic (Residual) Strain	0.2

4.4 Description of the FE Model under Monotonic Loading

4.4.1 Basic FE Model

The basic FE model was created with the concrete and Canam composite P-3623 steel sheet defined as a solid element and shell element, respectively as shown in Figures 4.6 and 4.7. In addition to the dimensions provided within the following figures, the total slab has a depth of 100 mm, the profiled concrete had a depth of 49 mm and the profiled steel sheet had the nominal thickness of 0.76 mm and total height of 51 mm (as per experimental slab).

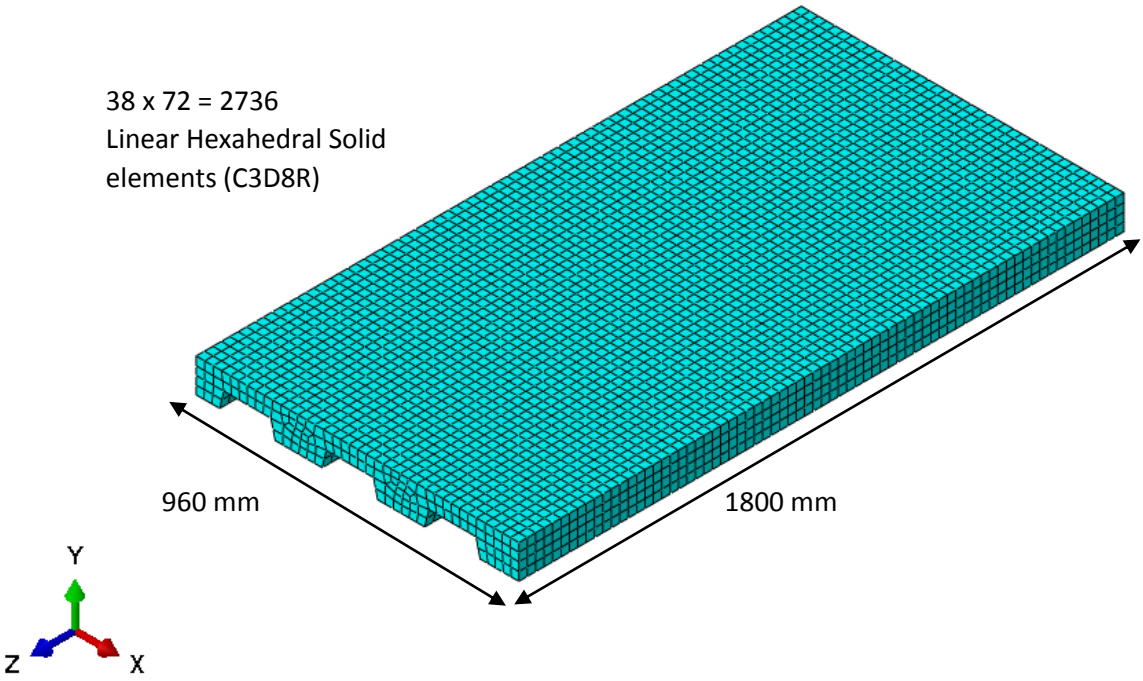

Figure 4.6: Meshing of profiled concrete using a linear 8-node brick (solid) element

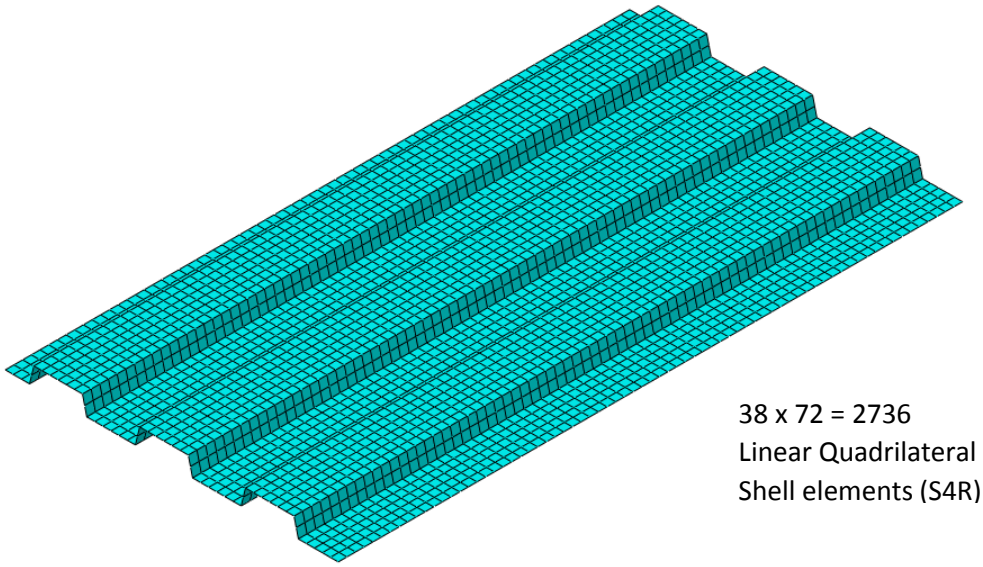

Figure 4.7: Meshing of Canam composite P-3623 steel sheet using linear 4-node shell element

In ABAQUS, the material properties for steel can be characterized as a homogeneous material. As concrete is a heterogeneous material with diversified mechanical properties, it is difficult to accurately define the concrete behaviour, thus for simplicity of FEA in this study, concrete is expressed as a homogeneous material.

The boundary conditions and prescribed transverse displacements of the composite slab are illustrated in Figure 4.8. The maximum out-of-plane deformation was applied along the depth of the slab (in Y-axis) with a linear prescribed displacement U2 (Uy) to simulate the bending deformation of the composite slab

associated with two-point loading. At the base of the profiled steel sheet, for the left-end roller support two displacement degrees of freedom (DOF) (U1 and U2) were restrained, and for the right-end pin support three all of the three displacement degrees of freedom (DOF) (U1, U2, U3) were restrained. For simulating the FE model behaviour closest to the experimental results, the roller and pin support were placed at a distance of 150 mm away from the edges of the composite slab and the two-point displacement load was applied at three different shear-span distances incuding, 300 mm, 450 mm, and 600 mm. The uniform displacement in Y direction at the top of the composite slab (as shown in Figure 4.8) was applied with an Amplitude function versus time. The Amp-1 is a function of horizontal and vertical displacement versus time, which can be defined as a smooth step tabular form in ABAQUS/CAE. The analysis was conducted with two steps defined as 'initial' and 'loading.'

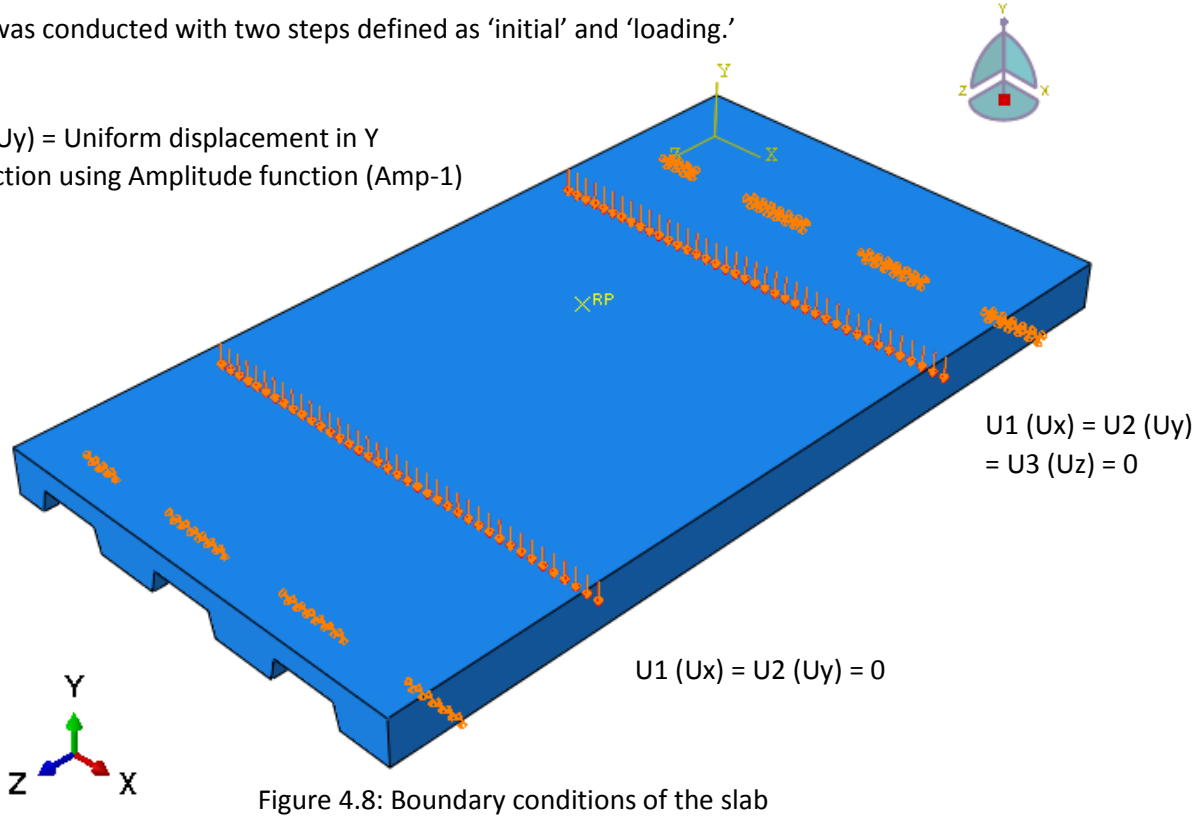

Figure 4.8: Boundary conditions of the slab

4.4.2 Parts, Meshing, and Element Assignment

As mentioned earlier, two parts (profiled concrete and composite P-3623 steel sheet) were created to make the finite element model of composite slab. Each of these two parts, including the meshing and assigned elements, was illustrated earlier in Figure 4.6 and Figure 4.7. These illustrations also indicate that the concrete was composed of linear hexahedral element (C3D8R) and respectively, the steel sheet was assigned the linear quadrilateral shell element (S4R).

Generally, using reduced integration for finite element analysis reduces the accuracy of the element; however it saves the computational cost. As the focus of this study is driven with displacement-based FE formulation, more integration points were used to produce a stiff element, however, this slightly increased the difficulty level of analysis interruptions. However, as this is a non-linear FEA of composite slab, using reduced integration rather than full integration improves the behaviour simulation of the composite slab with respect to experimental. Reduced integration uses a lower-order Gaussian integration to form the element stiffness. Figure 4.9 illustrates the location of the integration points for the two linear elements that were used in this FE model.

4-node reduced integration element (S4R) 8-node reduced integration element (C3D8R)

Figure 4.9: The integration points for linear elements (Rafiei 2011)

In ABAQUS/CAE, a default amount of artificial "hourglass stiffness" is utilized in linear reduced-integration elements to restrict the development of hourglass modes in the case when a large number of elements are used in the FE model. Thus, it allows the linear reduced-integration elements to provide reliable results with the help of using reasonably finer mesh size for the model parts. A brief description of the elements that were used in this basic FE model is presented in Table 4.3. A total of 12,528 elements were utilized to generate the entire FE composite slab model, with the breakdown of 8928 elements for concrete (C3D8R) and 3600 elements for profiled steel sheet (S4R).

Table 4.3: Description of stress/displacement elements

Element	Description
Linear Hexahedral element (C3D8R)	An 8-node linear brick element with reduced-integration and hourglass control. 3D stress family with uniform strain and linear geometric order. This element consists of only one integration point.
Linear Quadrilateral Shell Element (S4R)	A 4-node linear thick shell with reduced-integration and hourglass control. Shell family with uniform finite membrane strain and linear geometric order. This element consists of only single integration point.

Mesh refinement study was conducted in load and displacement control analyses to observe the variation in the results with changing mesh sizes, which is further discussed in Chapter 5.

4.4.3 Contact Surfaces

When the profiled concrete and steel sheet surfaces are in contact with each other, it generates a normal force that acts on the two contacting bodies at the points of interaction. The interface between concrete and steel sheet was characterized with penalty friction between these two surfaces, which generated shear forces to resist the tangential sliding motion of the two parts. In ABAQUS/CAE the interaction behaviour is a distinctive property which was specified to allow the transmission of forces between the profiled concrete and steel sheet surfaces. When subjected to two-point loading conditions, it was vital to define the interaction properties such that the slip failure due to separation of two contacting surfaces was minimized. The interface contact properties between the concrete and steel sheet were defined as follows:

- To produce a friction model that enables force resisting the relative tangential motion of the surfaces in the mechanical contact analysis, the 'tangential behaviour' was specified. Friction formulation field between the contact surfaces was selected as 'penalty' to allow some relative motion of the surfaces, for a uniform friction coefficient of 0.5 the directionality of 'isotropic' was chosen. Although the input of friction coefficient in the experimental analysis was slip-rate dependent, for the simplicity of the FE model it is not included.
- The normal contact behaviour for the interface was also defined as "Hard" contact for pressure-over-closure, and the "Default" constraint enforcement method was selected to enable the ABAQUS/Explicit analysis. Moreover, the separation of profiled concrete and steel sheet was prevented after these two surfaces came in contact with each other otherwise the model behaves as if no friction between the two surfaces was applicable, and thus, the two parts in the FE model do not demonstrate a composite behaviour.

The "Surface-to-surface contact" was utilized for interaction simulation in ABAQUS/Explicit, the first (master) surface was defined as concrete, and the composite P-3623 steel sheet was selected as second (slave) surface. For mechanical constraint formulation "Penalty contact method" was selected to use the penalty contact algorithm. "Finite sliding" formulation was also selected to allow any arbitrary motion of the concrete and steel sheet surfaces after slip failure between the two contacting surfaces. As a part of the parametric study, the influence of different mechanical constraint formulation and sliding formulation on the load-deflection curve was also evaluated in load control analysis. Based on which, it was learnt for a given two-point loading conditions, the Kinematic contact method with small or finite sliding formulation

generates the lowest maximum deflection at mid-span. However, for this FE model the penalty contact method is most suitable option for modeling the interaction between the concrete and steel sheet.

The following two chapters introduce the two FE models that were developed using ABAQUS/CAE (Explicit) to analyze the behaviour of composite slab by adopting “load control analysis” and “displacement control analysis”. In the first attempt, finite element analysis was performed with load control analysis. However, as further explained in Chapter 5, the load control failed to generate the expected elastic and plastic failure behaviour of the composite slab. As a result, the displacement control analysis was utilized to simulate reliable FE response, as introduced in Chapter 6. For each of the two types of analyses, the performance of the FE model was evaluated by changing multiple ABAQUS/CAE modeling parameters.

CHAPTER 5 – LOAD CONTROL FINITE ELEMENT ANALYSIS

5.1 Description of Model Setup

The two-point loading was applied to the surface of the concrete by defining two sets of nodes along the entire slab width of 960 mm and assigned a concentrated load that was uniformly distributed over all the selected nodes in the sets. The loading was defined in the negative Y direction (U2) towards the exterior concrete surface. The experimental load-deflection responses were for three different shear span locations - 300 mm, 450 mm, and 600 mm away from the supports that were located 150 mm away from the edges of the total span length. However, for the trial of load control analysis only 300 mm shear span distance was modeled in ABAQUS/CAE as the results were not feasible.

The boundary conditions defined for the roller and pin support of the steel sheet, as well as the material properties and interface contact properties were kept constant variables between load control and displacement control analyses. Although the experimental study was conducted on both Engineered Cementitious Composites (ECC) and Self-Consolidating Concrete (SCC), the provided Figure 5.1 presents the load-deflection behaviour comparison between the P3623-300-ECC-Experimental and P3623-300-ECC-FE Model. As a reference guideline, Table 5.1 presents the defined P3623-300-ECC-FE concrete material properties that was used to plot the load-deflection behaviour presented in Figure 5.1.

In Table 5.1, ψ represents the dilation angle in the p-q plane, ε is the flow potential eccentricity, σ_{b0}/σ_{c0} is the ratio of initial equibiaxial compressive yield stress to initial compressive yield stress, and *K*c represents the ratio of the second stress invariant on the tensile meridian.

Table 5.1: Concrete damaged plasticity and steel sheet input parameters for P3623-300-ECC finite element model

Steel	
Plasticity	
Yield Stress (MPa)	Plastic Strain (mm/mm)
230	0
251.3	0.000685
232.9	0.008125
313.2	0.093084
251.6	0.21

Concrete Damaged Plasticity			
Plasticity			
ψ	ε	σ_{b0}/σ_{c0}	*K*c
30	0.1	1.16	0.667
Concrete Compression Behaviour		**Concrete Compression Damage**	
Yield Stress (MPa)	Inelastic Strain (mm/mm)	Damage Parameter	Inelastic Strain (mm/mm)
30	0	0	0
50	0.0002	0.01	0.0001856
60	0.0008	0.02	0.0007650
45	0.0021	0.03	0.0020602
30	0.0029	0.04	0.0028643
Concrete Tensile Behaviour		**Concrete Tension Damage**	
Yield Stress (MPa)	Cracking Strain (mm/mm)	Damage Parameter	Cracking Strain (mm/mm)
30	0	0	0
0	0.0008	0.01	0.0002089
		0.02	0.0005042
		0.03	0.0008

5.2 Impractical ABAQUS Results using Load Control

The load-deflection response "P3623-300-ECC-FE Model" was plotted based on the results obtained from the load control analysis. This plotted curve in Figure 5.1 demonstrates that the load was gradually increased and the stiffness of the slab decreased with the increase of displacement until the peak load of 116.89 kN (at 24.61 mm displacement) and then the FE model shortly failed after reaching the mid-span displacement of 31.86 mm, which is illustrated with a cluster of points at the end of the curve. This sudden drop in the load and failure of the composite slab was observed with load control analysis possibly due to the formation of the major concrete crack. In comparison to the experimental curve, it can be concluded that by using the defined material and interaction properties was not sufficient to achieve the experimental results of ultimate peak load of 110.20 kN at a displacement of 14.27 mm; moreover, the similar initial stiffness for linear elastic load-deflection behaviour was not achieved for the ECC composite slab with load control analysis. After conducting an iterative model analysis by optimizing the material and contact interface properties for the profiled concrete and steel sheet, it was also learnt that the post-peak behaviour of the composite slab cannot be approximated with load control analysis due to the constant increase in load over the total duration of step time.

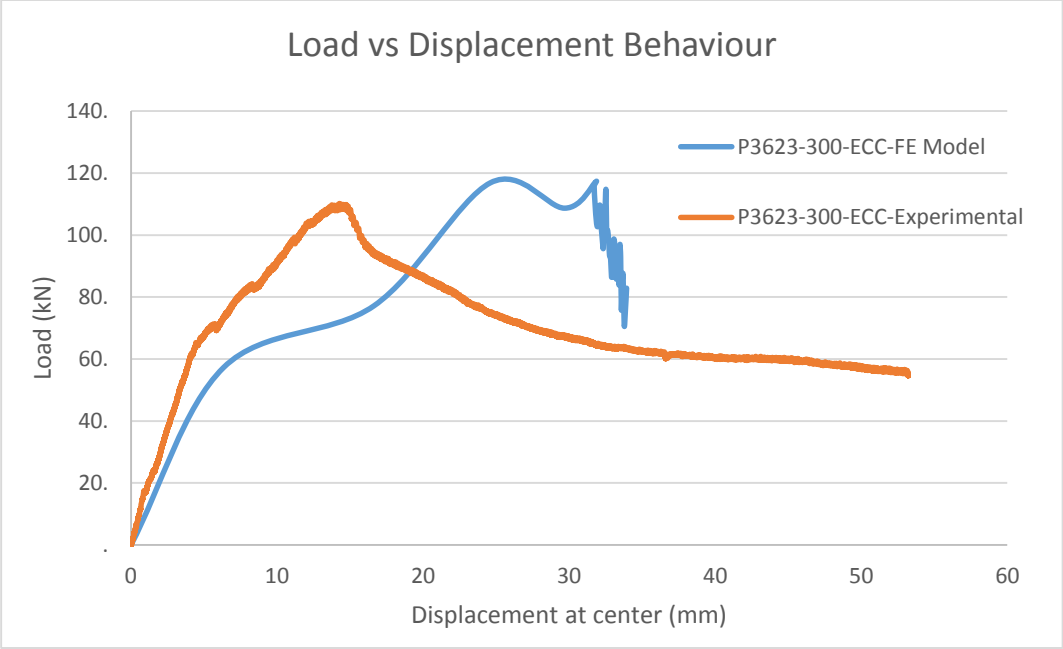

Figure 5.1: Load-deflection curve for load control analysis

In relation to the load-displacement curve presented, the following Figure 5.2 illustrates the difference between the original form and the deformed shape of that composite slab, as a response to the imposed two-point monotonic loading. Each of the two point loadings were divided into total of 78 nodes, with subdivision of 39 surface nodes across each loading width of the composite slab (along the X axis). Based on the spectrum of different colour contours, it can be concluded that the dark blue region represents the maximum failure displacement which has the magnitude of 45.62 mm. Hence, it is verified that using load control is not the best solution for controlling the maximum mid-span failure displacement or to achieve a post-failure response of composite slab, as proved in the following section.

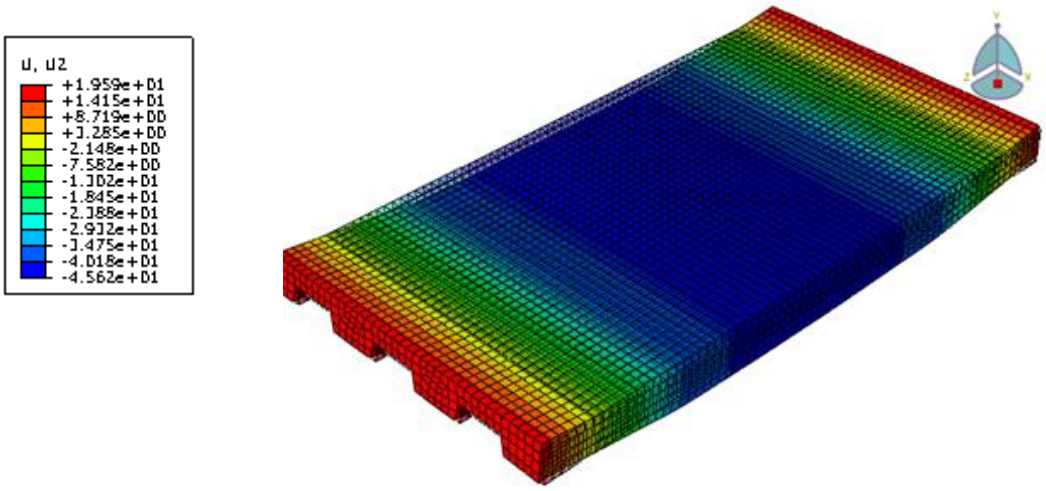

Figure 5.2: ABAQUS/Explicit load control model response to monotonic loading

5.2.1 Deficiency with Load Control Analysis

The following ABAQUS output curve illustrates the "Reaction force versus step time." Based on this graphs it can be verified that the sole objective of the load control analysis is to apply the total load consistently over the total defined step time of the job. Therefore, as shown in Figure 5.3 there is no drop in the force which is crucial to identify the load at which the composite slab fails, and obtain the post-failure of load-deflection curve. Load-control is most suitable for cyclic loading analysis or when the main objective is to determine the peak load that can be achieved by an experimental specimen. For this study, to determine the deflection response of composite slab under monotonic loading conditions, using displacement control is the most feasible analysis method.

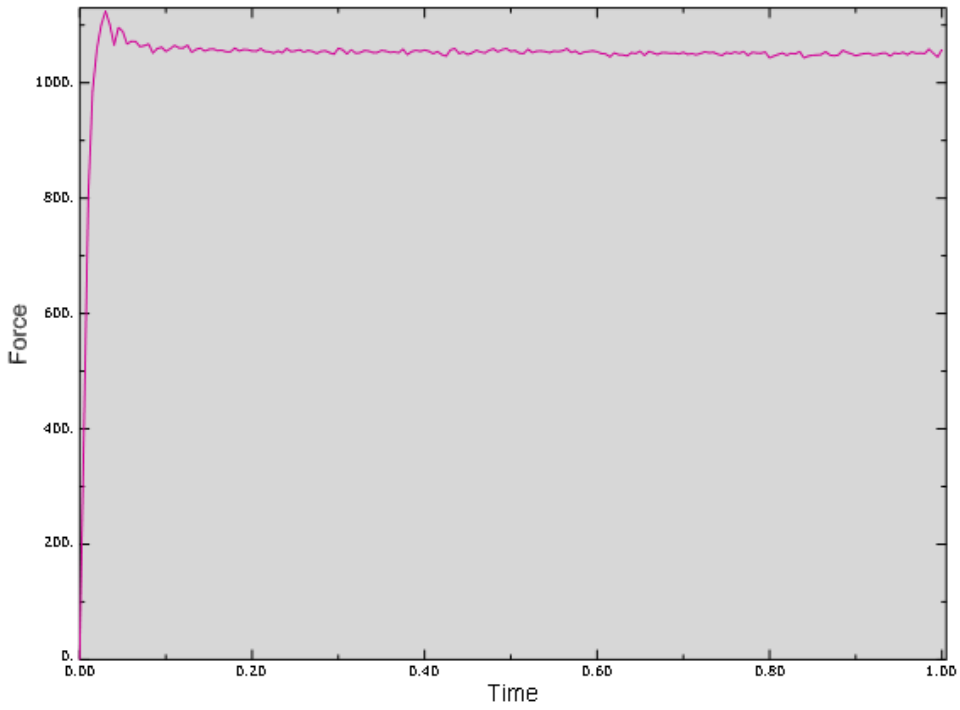

Figure 5.3: Load control - reaction force at roller support (N) versus step time (100%)

5.3 Parametric Study with Load Control Analysis

For load control analysis, the parametric investigation was performed by studying the effect of dilation angle and mesh element size on the behaviour of P3623-ECC composite slab. Based on the study of different dilation angles, the angle of 28 degrees was used to define the "Concrete Damage Plasticity (CDP)" model of ECC composite slab, and 35 degrees for SCC composite slab. Using these selected angles, reasonable simulation was achieved between the finite element and experimental slab behaviour.

Through the investigation of different mesh element sizes, the element size of 25 mm was used for nonlinear finite element modeling of both P3623-SCC and P3623-ECC composite slabs with displacement control analysis, as presented in following Chapter 6. Hence, in comparison to all mesh sizes, using 25 mm the simulation of load-deflection response was found to be closest to experimental curves.

5.3.1 Influence of Dilation Angle

Dilation angle is one of the plasticity input parameters for the concrete damage plasticity model that plays a crucial role in defining the three-dimensional surface of the concrete compression and tension damage behaviour in reference to the principal stresses axes. The defined compression yield stress with inelastic strain data table and the tension yield stress with cracking strain data table generate a 3D surface by using these plasticity parameters. If the software detects any error in producing such planes of stresses, the FE model fails to execute due to the development of negative eigenvalues. As a result of the lack of experimental material testing data, it was crucial to verify the effect of plasticity parameters on the load-deflection response of the composite slab.

As shown in Figure 5.4, increasing the dilation angle from 20 to 25 degrees caused the reduction in the magnitude of load that can be sustained by the composite slab to generate the same amount of displacement. The default value for dilation angle is 30 degrees. However, upon increasing that value to 35 degrees, it can be concluded that although both curves are capable of withstanding the same amount of imposed load, it increased the inconsistency with the post-cracking behaviour of the composite slab, which is possibly caused due to the interface slip between concrete and profiled steel sheet. The other potential advantage of increasing the dilation angle is that it slightly reduces the maximum displacement at the mid-span of the composite slab.

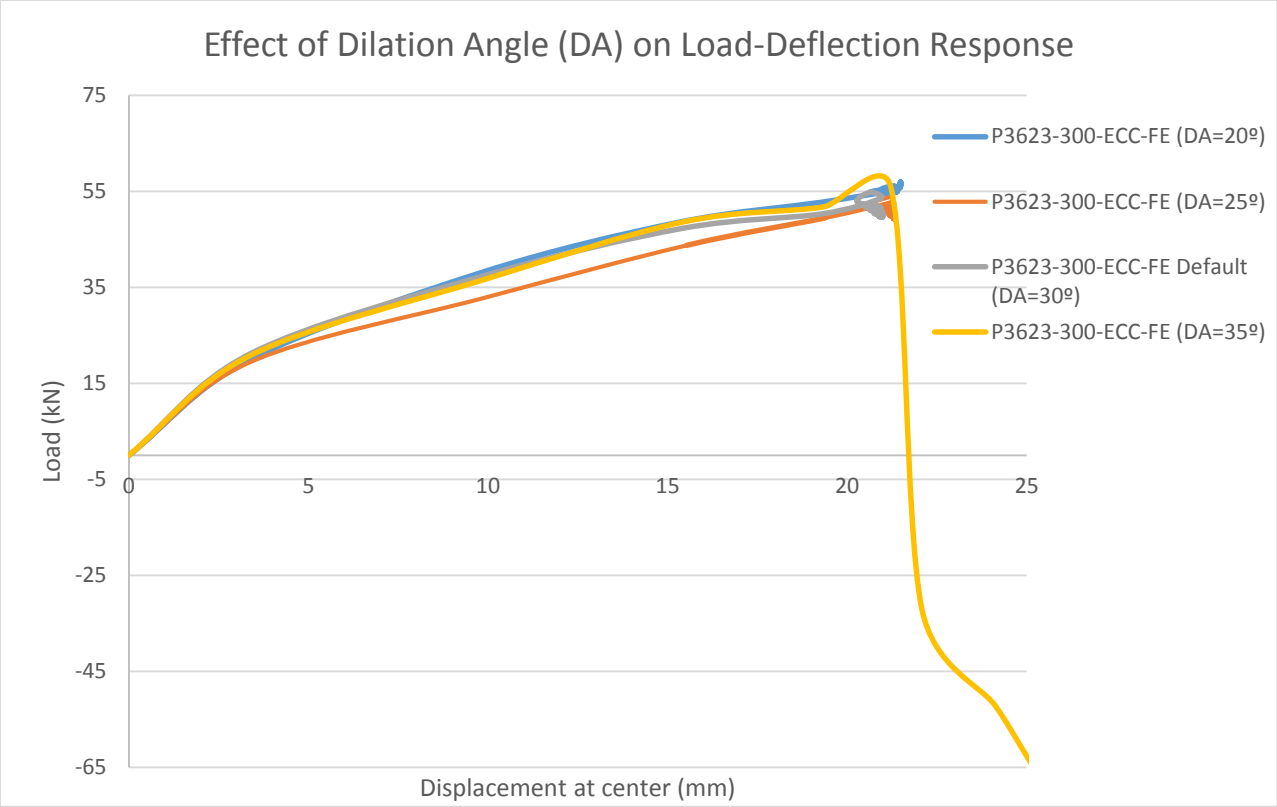

Figure 5.4: Load-deflection response for dilation angles in load control analysis

Based on the presented load-deflection curves in Figure 5.4, Table 5.2 provides a summary of the results obtained from parametric study conducted on dilation angle. The provided load and displacement ratio were calculated by using the experimental ultimate load of 110.20 kN and mid-span displacement of 14.27 mm. Based on the results presented in Table 5.2, it is confirmed that in order to achieve results close to experimental peak load, load control analysis is not a feasible approach as the maximum mid-span failure displacement will significantly increase and it must be controlled using displacement control analysis.

Table 5.2: Effect of dilation angle on load-deflection behaviour of P3623-ECC finite element (FE) model

Dilation Angle	FEA Ultimate Load (kN)	Experimental Load (kN)	FEA Mid-Span Displacement (mm)	Experimental Displacement (mm)	Load Ratio (Experimental/FEA)	Displacement Ratio (Experimental/FEA)
20	56.94	110.20	21.49	14.27	1.94	0.66
25	49.48	110.20	21.31	14.27	2.23	0.67
30	50.21	110.20	20.95	14.27	2.19	0.68
35	55.78	110.20	28.06	14.27	1.98	0.51

5.3.2 Mesh Sensitivity Analysis

In general, using finer size of mesh elements generates more accurate analyses results. It also produces more number of elements, due to which the computational cost increases with ABAQUS/CAE. However, this concept is not necessarily applicable for material such as composite slab due to the concrete softening concentration. It becomes difficult to overcome the persistent convergence problems that arise due to using smaller mesh element size. Thus, the best approach for meshing a FE model for composite slab is to use averagely small mesh element size (such as 20 mm) that generates reasonably uniform mesh for the entire model. For this study, the FE model for composite slab was designed with a mesh size of 25 mm for both parts of the composite slab, including concrete and steel sheet, although ABAQUS suggests that using a finer mesh for the master surface improves the accuracy of the model performance. It is also recommended to use ABAQUS/Explicit to resolve the specific convergence errors that are encountered with composite specimens.

Figure 5.5 illustrates the load-deflection response of the composite slab with three different mesh element sizes of 25 mm, 35 mm, and 50 mm. Based on the figure, it can be concluded that mesh refinement shortens the ductile response of the composite slab. The total load of 80 kN (divided in 40 kN per two-point loading) was modified with respect to each of the three mesh sizes as; 2000 N per node for mesh size of 50 mm, 1430 N per node for mesh size of 35 mm, and 1030 N per node for mesh size of 25 mm. However, the failing behaviour criteria for mesh optimization with load control analysis, based on the Figure 5.5, was that the capacity of the composite slab to withstand higher load should have increased by reducing the mesh element size. However, the graph depicts the complete opposite behaviour. Thus, it can be concluded that load control analysis is not feasible to analyze the load-deflection response of the composite slab.

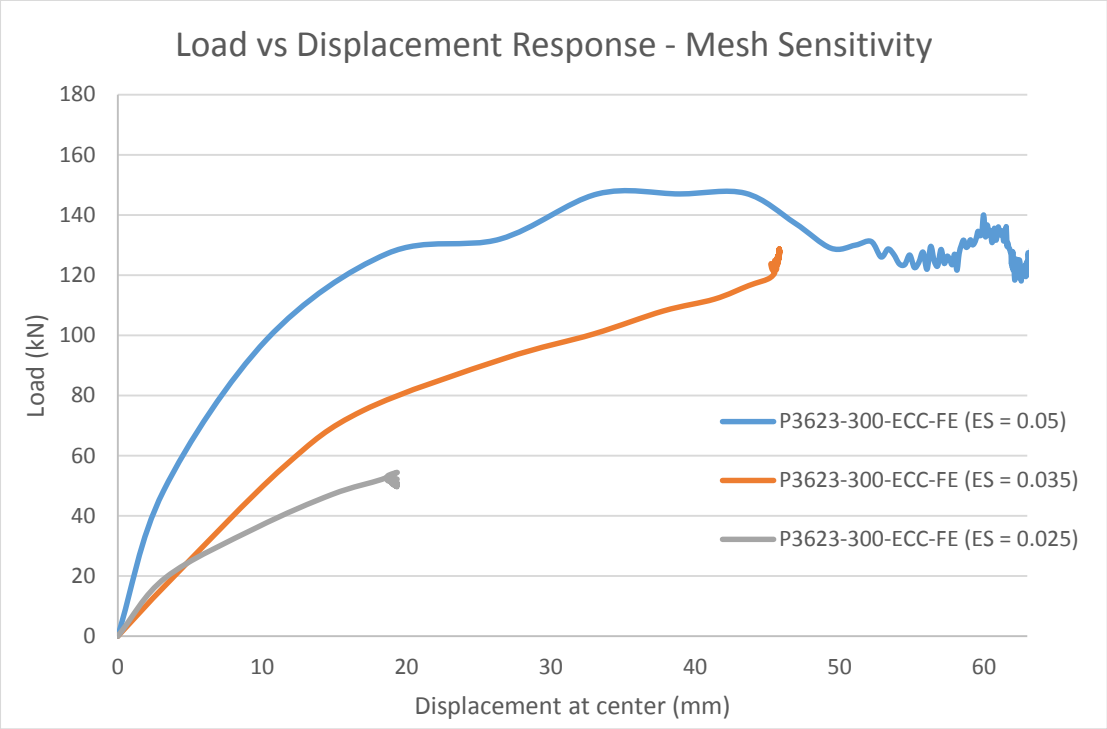

Figure 5.5: Mesh sensitivity study with load control analysis

Table 5.3 summarizes the results obtained from the parametric investigation carried out on mesh sensitivity. Similar to the previous study, the load and displacement ratio were calculated based on the experimental ultimate load of 110.20 kN and mid-span displacement of 14.27 mm. Table 5.3 verifies that the ultimate load capacity and failure mid-span displacement increased with the increase of mesh size in load control analysis. Table also depicts that as the mesh element size increased, the measure of accuracy between the finite element and experimental results also decreased.

Table 5.3: Effect of mesh element size (ES) on load-deflection behaviour of P3623-ECC FE model

Mesh Element Size	FEA Ultimate Load (kN)	Experimental Load (kN)	FEA Mid-Span Displacement (mm)	Experimental Displacement (mm)	Load Ratio (Experimental/FEA)	Displacement Ratio (Experimental/FEA)
0.025	50.47	110.20	19.29	14.27	2.18	0.74
0.035	128.68	110.20	45.85	14.27	0.86	0.31
0.05	147.28	110.20	63.01	14.27	0.75	0.23

CHAPTER 6 – DISPLACEMENT CONTROL FINITE ELEMENT ANALYSIS

6.1 Description of Selected FE Model for Monotonic Loading

The most suitable approach for conducting the finite element analysis of SCC and ECC profiled steel-deck composite slab using ABAQUS/Explicit is to utilize the "Displacement control" loading application. The loading was defined by specifying a Reference Point (RP) and assigning a prescribed displacement to the RP. The RP position was aligned by the center line of the composite slab span length, located 100 mm at the top of the specimen from the mid-span, as shown in Figure 6.1. The RP was constrained in the Y direction to the two sets of loading nodes across the whole width of the composite slab (in X direction). For parametric study of the composite slab under displacement control loading, different constraints were modeled to analyze which type is most feasible to simulate the load-deflection response closest to the experimental results. The prescribed displacement was defined by using amplitude function (smooth step) and uniform distribution in the boundary condition module. The position of RP was also changed to determine the response of the composite slab for the following three shear span distances from the centerline 300 mm, 450 mm, and 600 mm.

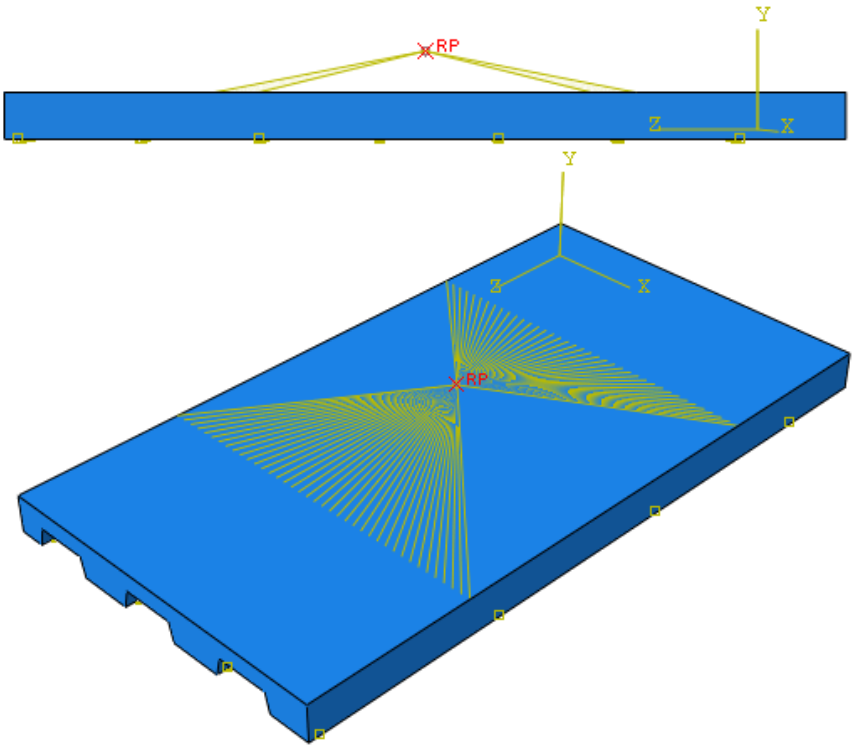

Figure 6.1: Location of the Reference Point (RP) and constraining the RP in Y direction to the two loading nodes at a shear span distance of 300 mm from support

Based on the parametric study results obtained from the load control analysis, the mesh size of 25 mm with dilation angle of 20° for SCC and 30° for ECC was used to develop the displacement control finite element model for the composite slabs in ABAQUS. In addition, the eccentricity in "Concrete Damage Plasticity" model was defined as 1.12 for SCC and 1.16 for ECC composite slab models, and the remaining parameters were constant as defined previously in load control analysis.

The analysis was conducted in step-1 (Dynamic, Explicit), which is a step after the initial step. Automatic increment and total of one second "Time period" were selected. A complete run of the ABAQUS/Explicit software for monotonic loading (1 second time period) using one of the basic available Personal Computers took 2.5 hours. The average stable time increment during analysis was 2.94859e-06 seconds.

6.2 Results from Displacement Control FE Analysis

For Displacement control analysis, the inelastic out of plane deformation for the entire span length of the P3623-ECC composite slab is portrayed in Figure 6.2. The maximum transversal displacement (U2 or Y direction) at the mid-span of the composite slab was determined as 16.00 mm when subjected to the two-point loading control across the top surface of the composite slab. The separation of the concrete and the profiled steel deck was also observed in the ABAQUS output, which was caused by the friction slip at the interface of the two elements, exhibiting the similar failure response to the experimental study.

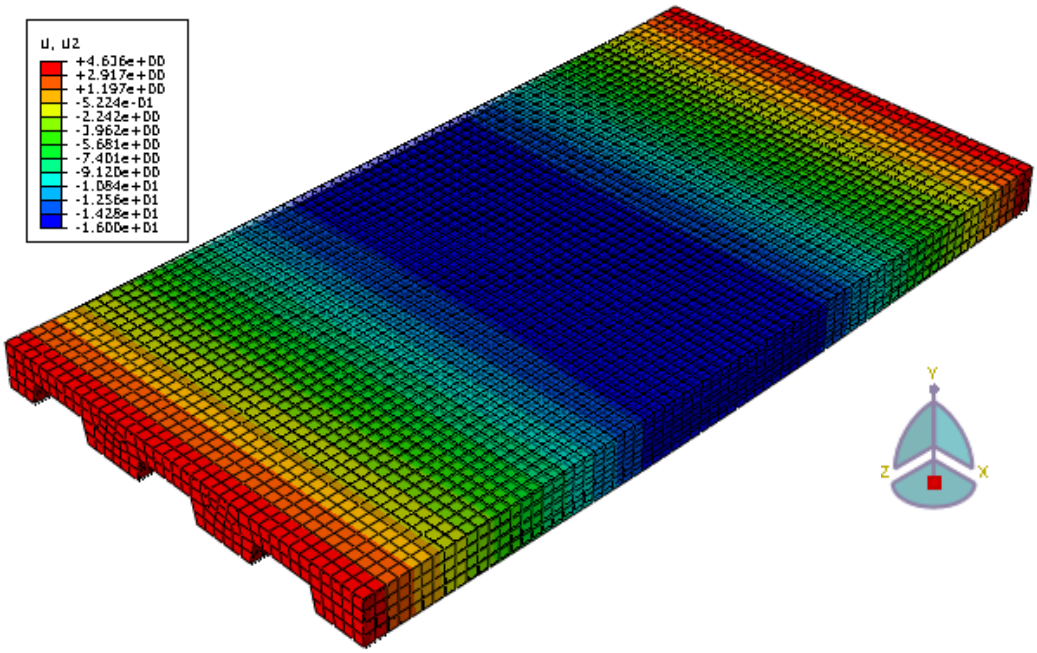

Figure 6.2: Typical deformed model output with ABAQUS/Explicit for shear span of 450 mm

The contour diagrams for the three principal stresses of the P3623-450-ECC composite slab, after reaching the maximum failure deformation, are shown in the following Figure 6.3. As illustrated, the concentration of the principal stress in X, Y, and Z direction is highest at the two shear span locations and progressively decreases towards the edges and the center of the composite slab and profiled steel deck. The failure mode of the FE model was initiated with the separation of the concrete and steel deck and lead by flexure failure due to the reduced tensile resistance, which was the primary function of the steel deck. Although the accuracy of the principal stresses from the FEA was affected by the defined interface friction contact property, it was verified that the ABAQUS model demonstrated similar failure performance to the experimental model.

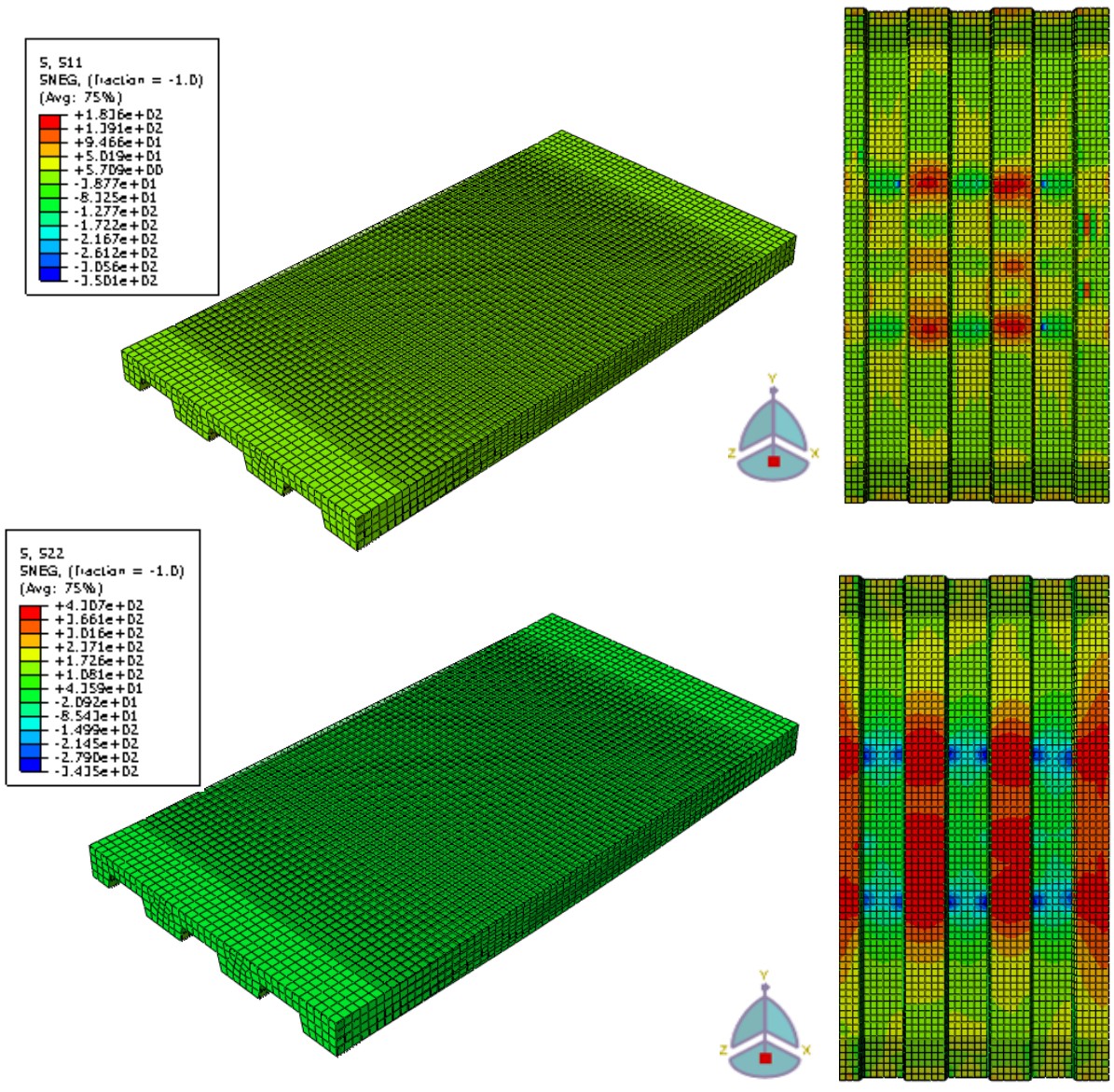

Figure 6.3: Contour of principal stresses in X, Y, and Z directions (MPa) for the composite slab and profiled steel sheeting after the application of two-point displacement control (contd.)

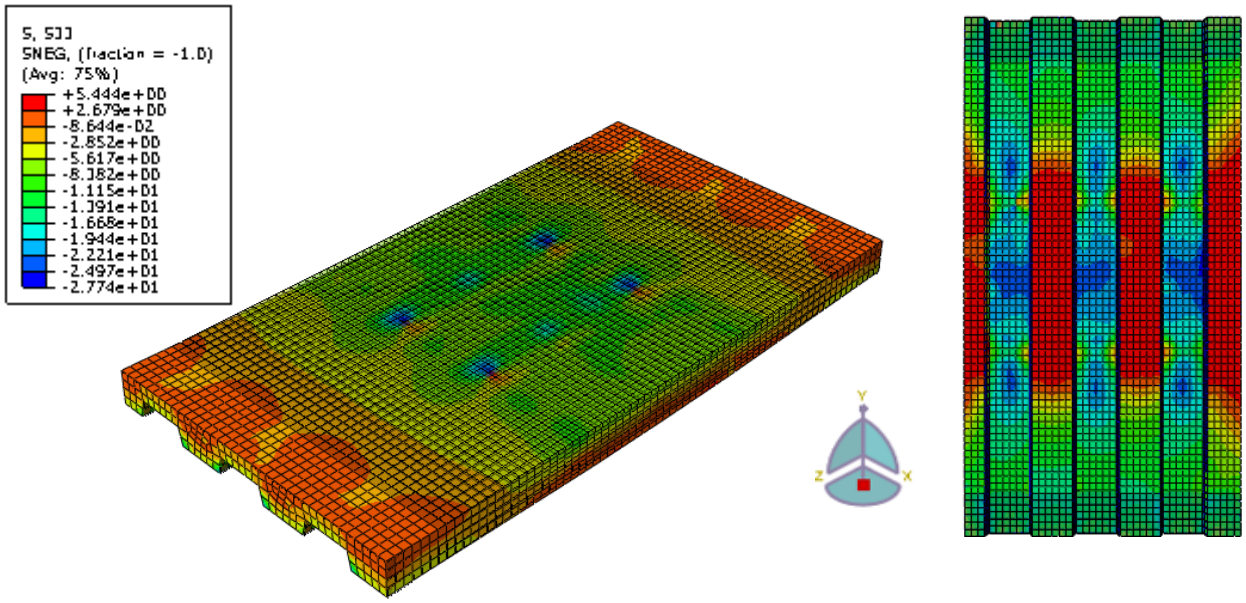

Figure 6.4: Contour of principal stresses in X, Y, and Z directions (MPa) for the composite slab and profiled steel sheeting after the application of two-point displacement control

According to Figure 6.3, P3623-450-ECC exhibits failure with uniformly distributed stress concentration of σ_{xx}= 38.77 MPa throughout the top surface of composite slab, and with small region of highest concentration of stress σ_{xx}= 183.6 MPa developed at the bottom of the ECC composite slab, along the shear span distances and at the mid-span location. In terms of stress in y direction, the composite slab experienced uniformly distributed stress concentration of σ_{yy}= 43.59 MPa throughout the top exterior surface. At the bottom of the slab, high stress concentration of σ_{yy}= 279.0 MPa was developed along the location of applied displacement control point loads; for the entire distance between the shear span locations where the profiled span length had a depth of 100 mm, high σ_{yy} stress concentration was developed ranging from 237.10 MPa to 430.70 MPa. The failure stresses in z direction (span length of the slab) was found to be the lowest of all three principal stresses, indicating that P3623-450-ECC composite slab had not completely yielded at failure point, due to which the magnitude of highest concentrated region of σ_{zz} = 27.74 MPa developed mostly throughout the region between the supports and shear span locations. The lack of stress development was potentially caused due to the early interface failure between P3623 steel sheeting and profiled ECC surface.

6.3 Comparison of FE Model Output with Experimental Results

6.3.1 Slab Load-Deflection Response of ECC composite slab

Figure 6.4 demonstrates the load-central displacement response of the finite element model of P3623-ECC composite slab model in comparison to experimental slabs for different shear spans of 300 mm, 450 mm, and 600 mm. As illustrated, there is relatively good correlation between the FE and experimental responses till the ultimate/peak load. Post peak failure response was not achieved because the stiffening effect after first tension cracking for ECC was not accurately defined or modeled in FE analysis. As part of further research, it is recommended to improve the accuracy of the nonlinear FE model by defining the post stiffening behavior of the ECC in the subroutine of the "Concrete Damage Plasticity" model.

The plotted curves verify that for a given slab span length of 1800 mm, the ultimate load capacity of the ECC composite slab was the highest (110.40 kN) for lowest shear span of 300 mm, and a significant reduction in load capacity was observed as the shear span increases to 450 mm (48 kN) and followed by the lowest ultimate load of 38.50 kN for shear span of 600 mm. According to the experimental curve, the first cracking and ultimate loads for ECC composite slab for a shear span of 300 mm were 16.33 kN and 110.20 kN, respectively compared to 17.56 kN and 110.40 kN, respectively for FE slabs. Based on the comparison of the ultimate load capacity, it can be concluded that the accuracy of FE models was excellent (less than 5% difference). A summary of this information is provided in Table 6.1.

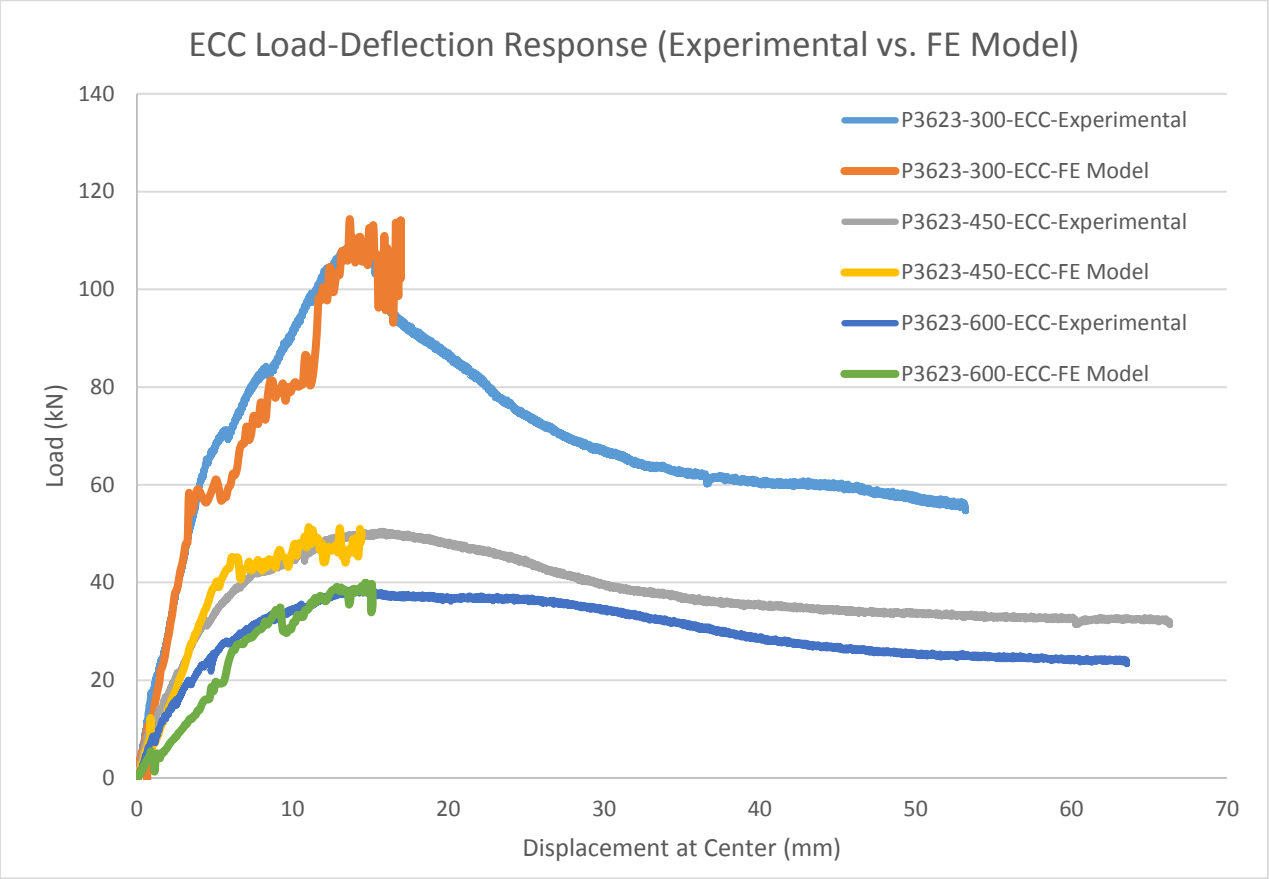

Figure 6.5: Comparison of experimental and FE load-displacement response ECC composite slabs

Based on the results provided in Table 6.1, it is observed that the accuracy of nonlinear finite element model of P3623-ECC was reasonably well in comparison to the results obtained from the experimental test results. Moreover, the load and displacement associated with first crack for each of the three shear span distances of ECC composite slab and total span length of 1800 mm falls within reasonable range of accuracy as well.

Table 6.1: Summary of load-displacement response for finite element (FE) model P3623-ECC

Specimen	FEA Ultimate Load (kN)	Experimental Load (kN)	FEA Mid-Span Displacement (mm)	Experimental Displacement (mm)	Exper./FEA Ratio		FEA First Crack		Experimental First Crack		First Crack Exper./FEA Ratio	
					Load	Displacement	Load (kN)	Displacement (mm)	Load (kN)	Displacement (mm)	Load	Displacement
P3623-300-ECC-	110.71	110.20	15.905	14.27	0.99	0.925	17.56	1.304	16.33	0.85	0.930	0.652
P3623-450-ECC-	51.08	50.54	15.203	15.83	0.99	1.041	8.59	0.707	9.89	0.76	1.151	1.075
P3623-600-ECC-	39.97	38.77	15.110	14.00	0.96	0.943	3.75	0.679	6.44	0.73	1.718	0.679

6.3.2 Load-Deflection Response of Self-Consolidating Concrete (SCC) Composite Slab

Figure 6.5 shows the comparison between the load-deflection curves for P3623-SCC composite slabs for the three shear spans. The linear pre-peak response was accurately matched between the experimental FE models. However, FE model failed to simulate the inelastic post-peak response possibly due to the inadequate modelling of interaction between the concrete and steel deck which was difficult to precisely define within ABAQUS/Explicit software. Another deficiency with this model was that the reinforcement detailing was not modeled within the FE model due to the modelling complication and it was taken into account within the “Concrete Damage Plasticity” model through increasing the tension stiffening. For future research purposes, it is recommended to also model the reinforcement in order to enhance the accuracy of nonlinear finite element model.

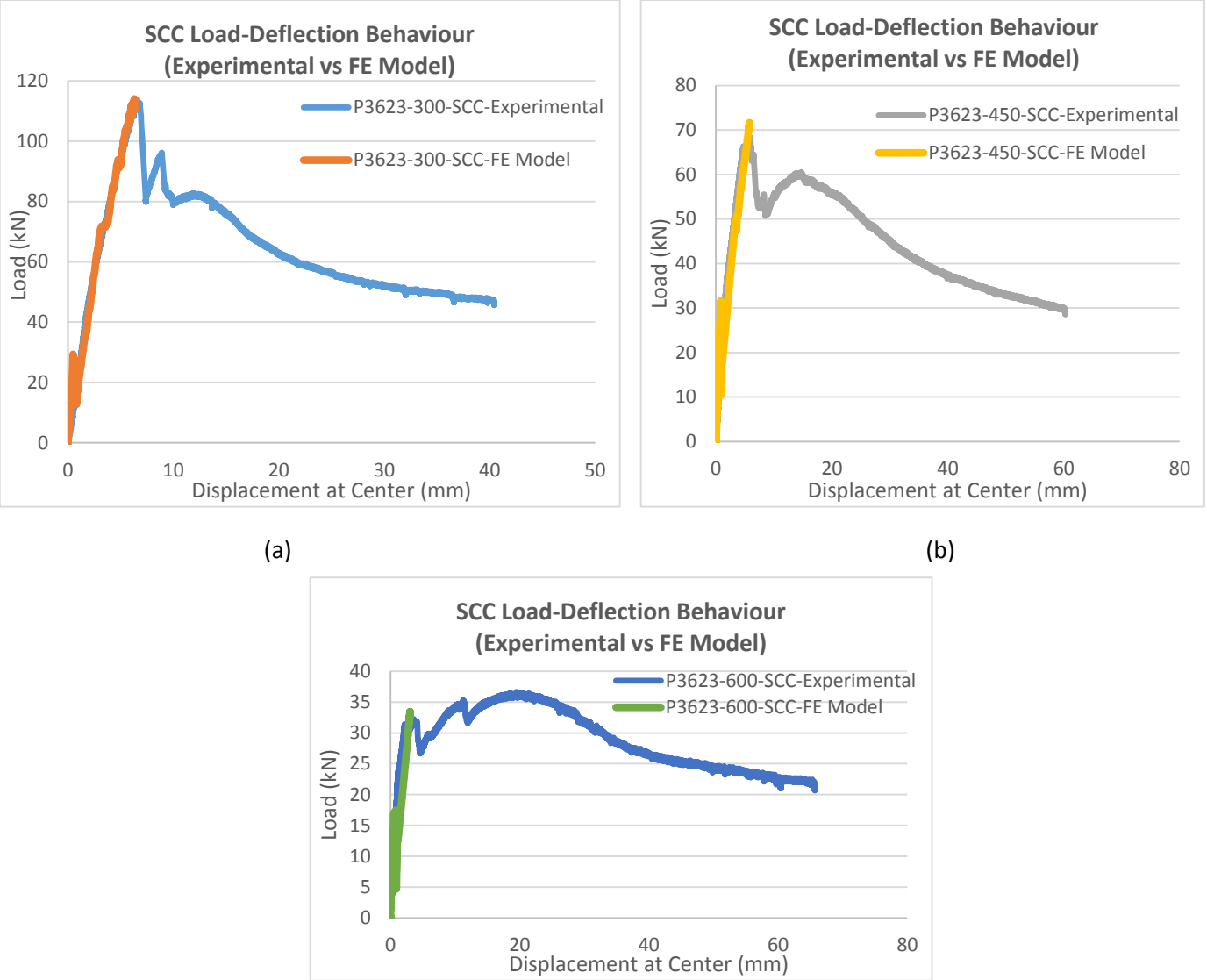

Figure 6.6: Comparison of experimental and FE load-displacement responses SCC composite slabs with shear span of (a) 300 mm, (b) 450 mm, and (c) 600 mm

Figure 6.5 shows that FE models accurately predicted the ultimate load of SCC slabs as the ratio of experimental to FE predicted values are close to 1. Based on the displacement comparison for two types of composite slabs, it can be concluded that ECC composite slab provides higher ductility (with approximately 40% higher mid-span displacement) with a slightly lower ultimate load capacity.

Table 6.2: Summary of results for finite element (FE) model of P3623-SCC load-displacement response

Specimen	FEA Ultimate Load (kN)	Experimental Load (kN)	FEA Mid-Span Displacement (mm)	Experimental Displacement (mm)	Experimental/FEA Ratio	
					Load	Displacement
P3623-300-SCC-FE Model	113.96	113.75	6.285	6.58	0.998	1.047
P3623-450-SCC-FE Model	71.40	68.43	5.781	5.82	0.958	1.019
P3623-600-SCC-FE Model	33.46	36.66	3.023	3.51	0.963	1.161

6.4 Finite Element Parametric Study of P3623-300-ECC Composite Slab

For conducting the parametric study with displacement control analysis, the load-deflection behaviour of P3623-300-ECC composite slab was analyzed for the following variables:

- Effect of different types of ABAQUS interaction properties, including kinematic – finite or small sliding, and penalty contact;
- Influence of different displacement loading constraint, such as coupling, MPC, and tie;
- Effect of using strain increment factor on concrete behaviour (tested with factor 1.5, 2, 2.5) and,
- Influence of increasing compressive strength of P3623-300-SCC (from f'c = 56 to 66 MPa)

Kinematic and penalty contact are two types of mechanical constraint enforcement methods that are used in ABAQUS/Explicit to model the pure master-slave surface interface contact. Finite sliding allows for any arbitrary motion of the two surfaces, whereas, small sliding assumes that although the two bodies may undergo large motions, there will be relatively little sliding of one surface along the other. In the case of composite slab where the interface slip is expected, small sliding is not feasible for FE modeling. Kinematic coupling is a rigid constraint between a reference node and the master surface nodes. Tie constraint provides permanent bonding between two surfaces (master-slave), thus, preventing the separation or sliding of the slave nodes in reference to master surface. Lastly, MPC, also known as multi-point constraint, imposed as a control point between a beam element and the slave surface nodes.

6.4.1 Effect of finite element model parameters on load-deflection behaviour

The response of P3623-300-ECC Composite slab was analyzed as a function of the different ABAQUS/Explicit modeling parameters and material properties. ECC composite slab load-displacement response for shear span of 300 mm was selected to perform this analysis. The variation of the load versus displacement curve in correspondence to the different ABAQUS interaction properties is presented in Figure 6.6. Based on the graph, it is verified that the "Penalty Contact" interaction provides the highest accuracy in simulating nearly identical load-deflection response as the experimental one. Using each of those three types of interaction properties results in approximately same slope for the linear (pre-peak) portion of the load versus displacement curve. For ECC composite slabs, "Kinematic Contact – Small Sliding" and "Penalty Contact" generated equivalent ultimate load capacity and maximum displacement at the mid-span. However, the ultimate load capacity is reduced significantly by using "Kinematic Contact – Finite Sliding" because this ABAQUS property accelerates the friction loss at the steel deck-concrete interface at a much earlier loading stage. Thus this form of interaction method is not feasible for profiled steel-deck composite slabs. It is also noted that the maximum deflection is roughly constant among all three types of interaction properties. However, pre-peak stiffness/slope, curvature of load-deflection response, and the ultimate load capacity of the composite slabs changed significantly for various contacts.

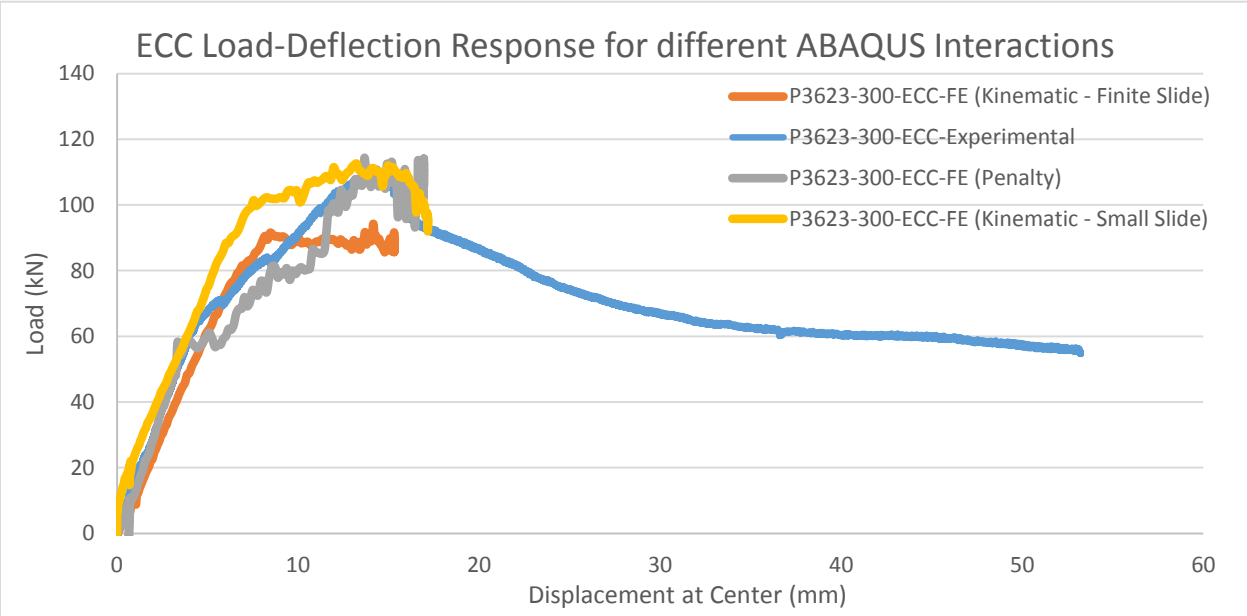

Figure 6.7: Load-displacement response of ECC composite slab for variable interaction property

Table 6.3 provides a summary of the results illustrated in the load-deflection curves shown in Figure 6.6. As stated in Chapter 5, the experimental ultimate load of 110.20 kN and mid-span displacement of 14.27 mm for P3623-300-ECC composite slab was utilized for measuring the accuracy of the nonlinear FE model results. Based on the tabular data, it is noted that the use of either of the three contact methods provides reasonably same accuracy in terms of the ratio of Experimental to FEA predicted values. However, using "Kinematic Contact with Small Sliding" generates the lowest magnitude of mid-span displacement with reasonably high peak ultimate load.

Table 6.3: Summary of the effect of ABAQUS interface properties on load-deflection response

Interaction Contact Property:	**FEA Ultimate Load (kN)**	**FEA Mid-Span Displacement (mm)**	**Experimental Load (kN)**	**Experimental Displacement (mm)**	**Load Ratio (Experimental/FEA)**	**Displacement Ratio (Experimental/FEA)**
Kinematic Contact - Finite Sliding	91.63	15.312	110.20	14.27	1.203	0.932
Penalty Contact	113.12	15.183	110.20	14.27	0.974	0.940
Kinematic Contact - Small Sliding	112.04	14.968	110.20	14.27	0.984	0.953

Figure 6.7 illustrates how the load-deflection behaviour of the P3623-300-ECC-FE composite slab varies based on the application of three ABAQUS displacement control loading constraints namely coupling, MPC, and tied. The figure proves that using "Coupling Constraint" for ABAQUS FE modeling is the most suitable load control approach for simulating the load versus displacement response of the ECC composite slab. Based on the Figure, it is also learnt that both MPC and Tie Constraints demonstrate similar load-displacement relationship with the same ultimate load and mid-span displacement. However, it is not feasible to correspond with the experimental results as the slope of linear portion of the curve, maximum displacement, and ultimate peak load point does not match. This significant difference between the "Coupling" and the other two constraints was caused due to the different behavioural characteristics of these constraints that change the imposed displacement control loading. Hence, this parametric study also reveals that the selection of the ABAQUS FE modeling features should be based on the objective of simulating the experimental behaviour.

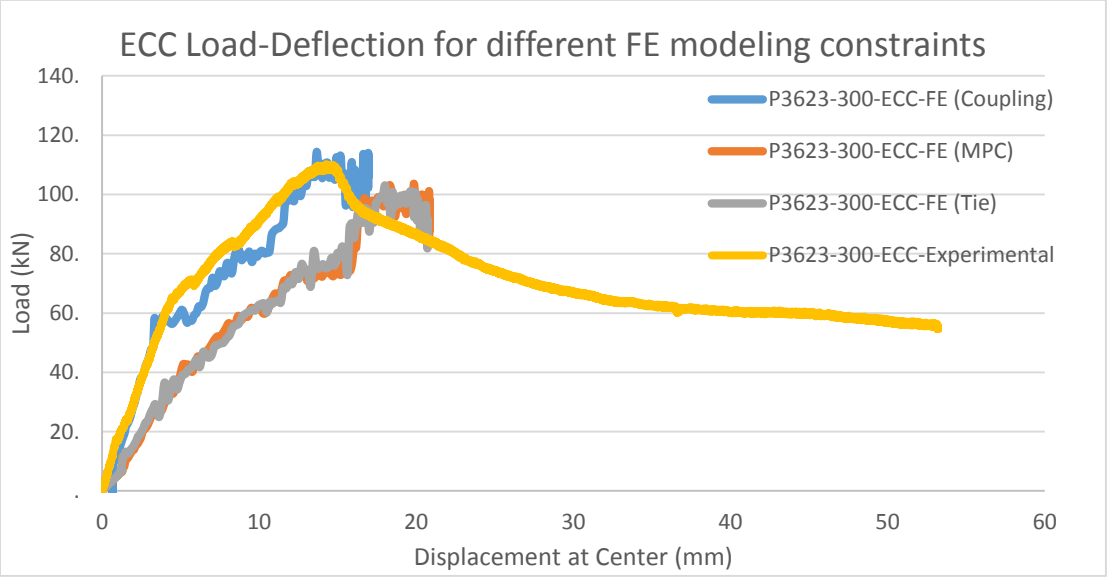

Figure 6.8: Load-displacement responses of ECC composite slab with displacement loading constraints

The load-deflection results illustrated in Figure 6.7 are briefly summarized in the Table 6.4. The presented tabular data emphasize that among all three types of constraints, coupling generates the highest ultimate peak/failure load. Although the ultimate load capacity is approximately same for both MPC and tie constraints, MPC generates higher mid-span displacement in comparison to coupling and tie constraints. Hence it can be concluded that with coupling constraint, the maximum mid-span displacement can be controlled to achieve the desired ultimate load capacity.

Table 6.4: Summary of the effect of loading constraints on load-deflection behaviour

Displacement Loading Constraints:	**FEA Ultimate Load (kN)**	**FEA Mid-Span Displacement (mm)**	**Experimental Load (kN)**	**Experimental Displacement (mm)**	**Load Ratio (Experimental/FEA)**	**Displacement Ratio (Experimental/FEA)**
Coupling Constraint	114.37	16.95	110.20	14.27	0.963	0.842
MPC Constraint	103.55	19.85	110.20	14.27	1.064	0.719
Tie Constraint	103.015	18.02	110.20	14.27	1.070	0.792

As another part of the parametric study for P3623-300-ECC composite slab, the influence of defined material properties on the load versus displacement response was analyzed. For the “Concrete Damage Plasticity” model in ABAQUS/CAE, the concrete cracking strain in tension behaviour for SCC composite slab represented the standard “Strain Increment Factor of 1.0. Based on that, the cracking strain for ECC

composite slab was increased by a factor of 1.5, 2.0, and 2.5 to observe the variation in the load-deflection response. Based on Figure 6.8, use of the "Strain Increment Factor of 2.0" yields better simulation in terms of ultimate load and maximum displacement. It is also implied that as the increment factor for cracking strain values becomes larger, higher ultimate load capacity is achieved for a given displacement. Moreover, the maximum displacement at ultimate load is also reduced with higher strain increment factor. In practice, this strain increment approach was adopted to model the "Concrete Damage Plasticity" for ECC due to the lack of available experimental data that made it difficult to achieve the accurate concrete compression and tension damage behaviour. However, for future research it is recommended that precise inelastic strain, cracking strain, and yield stress values should be developed to define the nonlinear post-stiffening performance of FE composite slab model that is composed ECC.

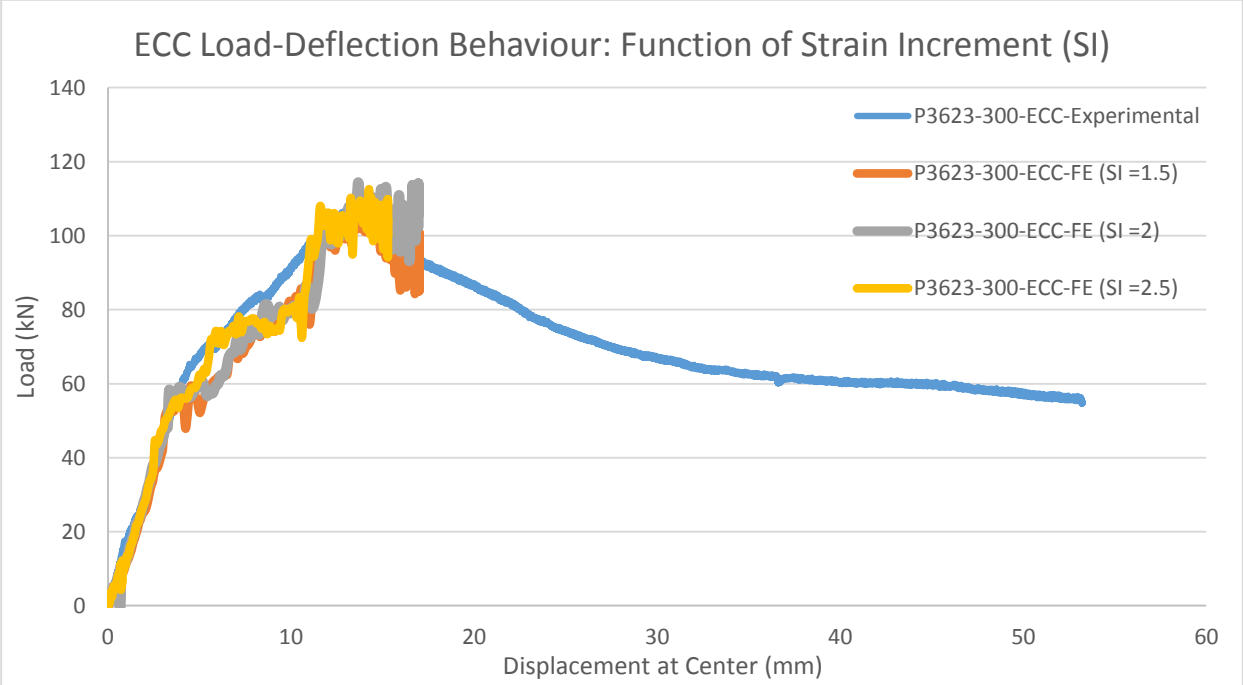

Figure 6.9: Load versus displacement behaviour of ECC composite slabs as a function of strain increment

Table 6.5 provides a summary of the results presented via load-deflection curves in Figure 6.8. The tabular information validates the fact that when the tensile strain values of ECC are increased by a factor of 2.0 it generates the highest ultimate load and lowest maximum mid-span failure displacement compared to 1.5 and 2.5. However, with factor of 2.5, the curvature of load-deflection response is closer to the experimental curve. Hence, composite slabs having different shear spans were modelled and found that

the tensile strain increment of 2.0 was the most feasible factor for simulating the nonlinear finite element behaviour of P3623-ECC composite slab.

Table 6.5: Effect of strain increment (SI) factor on load-deflection behaviour

Strain Increment Factor:	FEA Ultimate Load (kN)	Experimental Load (kN)	FEA Mid-Span Displacement (mm)	Experimental Displacement (mm)	Load Ratio (Experimental/FEA)	Displacement Ratio (Experimental/FEA)
1.5	109.02	110.20	14.403	14.27	1.007	1.022
2	114.38	110.20	13.671	14.27	0.960	1.077
2.5	112.19	110.20	14.266	14.27	0.978	1.032

For displacement control analysis, the last parametric study was performed on both P3623-300-SCC and P3623-300-ECC FE composite slab models to, compare the load versus displacement response when both materials had concrete compressive strength of 66 MPa. Hence, for compressive behaviour of both SCC and ECC in the “Concrete Damage Plasticity” model was developed by defining the same chart of yield stress values for different inelastic strain values. The orange curve in Figure 6.9 illustrates that the use of 66 MPa (in comparison to f’c of 56 MPa) allowed SCC slab to achieve higher ultimate load for the same maximum displacement of 6.13 mm, thus, improving the performance of the SCC composite slab. In comparison to ECC, the ultimate load capacity (7.68 kN) of SCC composite slab was higher with maximum displacement of 7.51 mm at the peak load less than ECC slab. However, the plotted curves also verify that the ductility of ECC composite slab is was significantly higher as confirmed from the gradual decline in the post peak load with the increase of displacement. It is also verified that the pre-peak stiffness of both SCC and ECC composite slabs were identical.

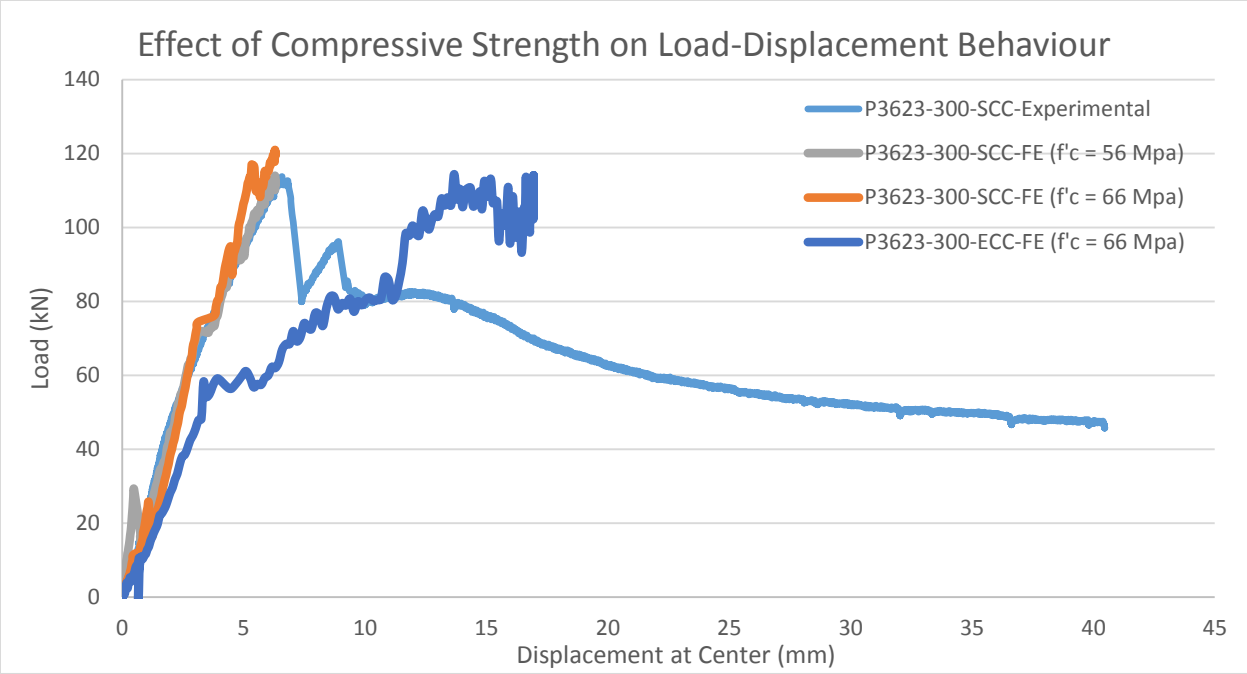

Figure 6.10: Comparison of load-displacement behaviour of SCC and ECC composite slab for constant concrete compressive strength

Table 6.6 provides a summary of the main results that are obtained for P3623-300-SCC finite element model. An increase of the compressive strength of SCC did not improve the maximum mid-span failure displacement. This can be attributed to the increased brittleness of SCC at higher compressive strength.

Table 6.6: Summary of results for P3623-300-SCC FE model for different compressive strength

SCC Compressive Strength f'c (Mpa)	FEA Ultimate Load (kN)	Experimental Load (kN)	FEA Mid-Span Displacement (mm)	Experimental Displacement (mm)	Load Ratio (Experimental/ FEA)	Displacement Ratio (Experimental/ FEA)
56	113.96	113.75	6.284	6.58	0.998	1.047
66	120.94	113.75	6.289	6.58	0.941	1.046

6.4.2 Summary

According to parametric studies, the “penalty contact method” provided the best simulation of experimental load-deflection behaviour among other interface contacts. Among the different displacement loading constraints, the use of “coupling constraint” was the only suitable approach for simulating reasonable composite slab response. Through comparison of different strain increment factors, it was observed that the use of tensile strain increment of 2.0 provides highest accuracy in

simulating load-deflection behaviour of P3623-300-ECC composite slab. Lastly, increase of concrete compressive strength of P3623-300-SCC slab from 56 MPa to 66 MPa was able to achieve a higher peak load with slightly lower mid-span displacement. However, the slope/stiffness of the pre-peak load-deflection curve remained unchanged.

6.5 Design Implementation of Developed FE Models

The developed FE models were used to simulate the behavior of a number of ECC and SCC numerical slabs having variable spans under four point loading static monotonic loading. The results obtained from such simulations are summarized and presented in the following sections in terms of ultimate load capacity, mid-span displacement, and moment resistance capacity as a function of different span lengths (1500 mm, 1800 mm, and 2100 mm) of P3623-ECC-FE and P3623-SCC-FE composite slab models. For each span length, a constant ratio of shear span distances was used to compare the behaviour of composite slab. The results of these numerical slabs are used to determine the moment resistance and shear bond capacity of the composite slabs using m-k method. ECC composite slab exhibited better shear resistance compare to their SCC counterparts with the increase of span. The detail data from FE simulations are also presented in Appendices.

6.5.1 Comparison of the Moment Resistance with Span

The behavior of P3623-ECC and P3623-SCC numerical composite slabs were simulated under four pointed loading using developed FE models for different span lengths (provided in Table 6.8) while keeping constant ratio of shear span distances as 1/6, 1/4, and 1/3 of the total span length following the design table produced by CANAM Group. The factored load resistance (uniformly distributed load ‘w’) of these slabs for a concrete compressive strength (f’c) of 20 MPa was provided in Canam Group 2006 catalogue for P3623 composite slabs. Table 6.7 presents the calculated moment and deflection values as per CANAM catalogue. However, these factored resistance values based on CANAM catalogue can be compared with FE model resistance as the concrete compressive strength of 20 MPa is significantly lower than 56 MPa (for SCC) and 66 MPa (for ECC). Hence for design purposes, the ultimate load capacity, failure mid-span displacement and the moment capacity of FE model composite slabs (P3623-ECC and P3623-SCC) having total span lengths ranging from 1500 mm to 2700 mm with three different shear spans are presented in Table 6.8.

Table 6.7: Factored resistance for CANAM P-3623 composite slab as per CANAM design catalogue

CANAM P-3623 Specified Standards:				
Total Span Length (mm)	1500	1800	2100	2700
Factored Load w (kPa) for f'c = 20 MPa	20.00	16.05	12.20	7.87
Moment Resistance (kNm) for f'c = 20 MPa	5.63	6.50	6.73	7.17
Deflection Limit (mm) using w_f for f'c = 20 MPa	1.14	1.89	2.66	4.69

For both SCC and ECC composite slabs, the ultimate load and moment resistance decreased with the increase of total span length. On the other hand, the ultimate load and moment resistance generally increased with the decrease of shear span for all composite slab. Although the ultimate peak load and moment capacity were higher for SCC composite slab, ECC composite slabs exhibited superior ductile performance.

Table 6.8: Comparison of the ultimate moment resistance with ABAQUS FE model results

ABAQUS FE Model Results – P3623-ECC Composite Slab:												
Total Span Length (mm)	1500			1800			2100			2700		
Shear Span Distance (mm):	250	375	500	300	450	600	350	525	700	450	675	900
Ultimate Load Capacity (kN):	152.54	98.74	80.90	110.40	50.77	39.48	100.27	47.89	36.63	86.98	37.42	27.10
Uniformly distributed force (w): (kPa)	105.93	68.57	56.18	63.89	29.38	22.85	49.74	23.76	18.17	33.56	14.44	10.45
Moment Resistance (PL/4) (kNm) for f'c = 66 MPa	57.20	37.03	30.34	49.68	22.84	17.77	52.64	24.14	19.23	58.71	25.26	18.29
Moment Resistance ($\frac{wl^2}{8}$) (kNm) for f'c = 66 MPa	29.79	19.28	15.80	25.88	11.90	9.25	27.42	13.10	10.02	30.58	13.16	9.526
Deflection (mm)	16.56	14.86	15.11	16.95	15.01	15.11	18.02	16.42	16.50	18.57	17.79	15.47
ABAQUS FE Model Results – P3623-SCC Composite Slab:												
Total Span Length (mm)	1500			1800			2100			2700		
Shear Span Distance (mm):	250	375	500	300	450	600	350	525	700	450	675	900
Ultimate Load Capacity (kN):	197.62	133.78	90.32	113.0	70.65	31.11	104.58	55.94	27.77	79.92	44.03	20.27
Uniformly Distributed Force (w): (kPa)	137.23	92.90	62.72	65.39	40.89	18.002	51.87	27.75	13.78	30.84	16.99	7.82
Moment Resistance (PL/4) (kNm) for f'c = 56 MPa	74.11	50.17	33.87	50.85	31.79	13.998	54.90	29.37	14.58	53.95	29.72	13.68
Moment Resistance ($\frac{wl^2}{8}$) (kNm) for f'c = 56 MPa	38.60	26.13	17.64	26.49	16.58	7.29	28.60	15.30	7.59	28.10	15.48	7.13
Deflection (mm)	5.91	5.56	3.09	6.28	5.78	3.05	8.16	7.12	3.42	8.31	6.42	3.42

6.5.2 Evaluation of shear bond characteristics for composite slabs

The results from the simulation of numerical slabs presented in Table 6.8 were used to determine the m and k values, defining the shear transferring capacity of the profiled composite deck. The variable "*m*" represents the empirical value of mechanical interlocking between concrete and profiled steel sheeting, the parameter "*k*" is the empirical value for friction at the interface of concrete and steel deck, and $\tau_{u,Rd}$ represents the shear bond capacity of the ECC and SCC composite slabs. Table 6.9 provides the calculated value of m, k, and $\tau_{u,Rd}$ for four different span lengths 1500 mm, 1800 mm, 2100 mm, and 2700 mm. Numerical slabs with each of these span lengths were modeled for three different shear spans maintaining a constant shear span to total span length ratio.

The main objective of this finite element analysis was to compare the shear bond capacities of SCC and ECC composite slabs. The design equation recommended by Porter et al. (1971) and Eurocode 4 (1994) for shear bond capacity (based on m and k values) of profiled steel deck composite slab is utilized for numerical and experimental composite slabs. Bashar (2010) and Marimuthu et al (2007) also used this method to determine the m-k values. The equation used in this method is given by Eq. 6.1.

$$\frac{V_u}{bd} = \tau_{u,Rd} = m\frac{A_p}{bL_s} + k\sqrt{f_c^{'}} \tag{6.1}$$

The provided Eq. 6.1 can also be rearranged in the format y = mx + b as Eq. 6.2:

$$\frac{V_u}{bd\sqrt{f_c^{'}}} = m\frac{A_p}{bL_s\sqrt{f_c^{'}}} + k \tag{6.2}$$

Where V_u is the ultimate shear capacity of the slab which is equivalent to $P_u/2$, P_u being the two load in four point loading, b is the width of the profiled sheet (given as 914 mm), d is the average depth of the composite deck slab (calculated as 75 mm), A_p represents the cross sectional area of the profiled steel sheet (given as 1016 mm^2), L_s is the shear span, and $f_c^{'}$ is the concrete compressive strength (used as 56 MPa for SCC and 66 MPa for ECC).

Numerical and experimental results are plotted in Figure 6.10 to determine m and k values. M and k values are determined as slope and intercept, respectively from the best fit straight line as per Eq. 6.2.

Then the following Eq. 6.3 was used to calculate the shear bond capacity of the composite slabs for different shear span distances:

$$\tau_{u,Rd} = \left(\frac{mA_p}{bL_s} + k\sqrt{f_c^{'}} \right) \tag{6.3}$$

The discussed parameters for calculating shear bond capacity of experimental and numerical composite slabs (ECC/SCC) are presented in Tables 6.9 and 6.10, respectively. Shear bond capacity of ECC and SCC composite slabs decreased with the increase of shear span.

Table 6.9: Experimental m-k values and shear bond capacity

Concrete Type	Span Length (mm)	Shear Span, Ls (mm)	Pu (kN)	Vu (kN)	$V_u / bd\sqrt{f_c^{'}}$	$A_p / bL_s\sqrt{f_c^{'}}$	m	k	$\tau_{u,Rd}$ (N/mm^2)
P3623-ECC	1800	300	110.20	55.10	0.0942	0.000434	291.38	0.0345	1.3085
		450	50.54	25.27	0.0432	0.000289			0.9658
		600	38.77	19.39	0.0331	0.000217			0.7945
P3623-SCC	1800	300	113.75	56.88	0.1056	0.000471	298.38	0.0339	1.3063
		450	68.43	34.22	0.0635	0.000314			0.9554
		600	36.66	18.33	0.0340	0.000236			0.780

Table 6.10: Parameters to plot finite element (FE) m-k curves, and shear bond capacity

Concrete Type	Span Length (mm)	Shear Span, Ls (mm)	Pu (kN)	Vu (kN)	$V_u / bd\sqrt{f_c'}$	$A_p / bL_s\sqrt{f_c'}$	m	k	$\tau_{u,Rd}$ (N/mm^2)
P3623-ECC-FEA Model	1500	250	152.537	76.269	0.13039	0.000521	239.29	0.00459	1.050284
		375	98.735	49.368	0.0844	0.000347			0.712619
		500	80.895	40.448	0.06915	0.000261			0.543787
	1800	300	110.40	55.20	0.09437	0.000434	289.63	0.033662	1.295218
		450	50.765	25.383	0.0434	0.000289			0.954635
		600	39.482	19.741	0.03375	0.000217			0.78434
	2100	350	100.269	50.135	0.08571	0.000372	302.12	0.02856	1.145586
		525	47.894	23.947	0.04094	0.000248			0.841068
		700	36.625	18.313	0.03131	0.000186			0.688809
	2700	450	86.98	43.490	0.07435	0.000289	365.84	0.03332	1.131107
		675	37.423	18.712	0.03199	0.000193			0.844306
		900	27.096	13.548	0.023162	0.000145			0.70091
P3623-SCC-FEA Model	1500	250	197.617	98.809	0.18339	0.000566	346.62	0.01117	1.550911
		375	133.781	66.891	0.12415	0.000377			1.061791
		500	90.319	45.160	0.08382	0.000283			0.817232
	1800	300	113.0	56.50	0.104863	0.000471	312.08	0.03982	1.398963
		450	70.65	35.325	0.065563	0.000314			1.031980
		600	31.107	15.554	0.02887	0.000236			0.84849
	2100	350	104.575	52.288	0.09704	0.000404	350.25	0.04397	1.388140
		525	55.936	27.968	0.05191	0.000269			1.035111
		700	27.772	13.886	0.02577	0.000202			0.858596
	2700	450	79.924	39.962	0.07417	0.000314	347.37	0.03423	1.07315
		675	44.029	22.015	0.04086	0.00021			0.800824
		900	20.272	10.136	0.01881	0.000157			0.664664

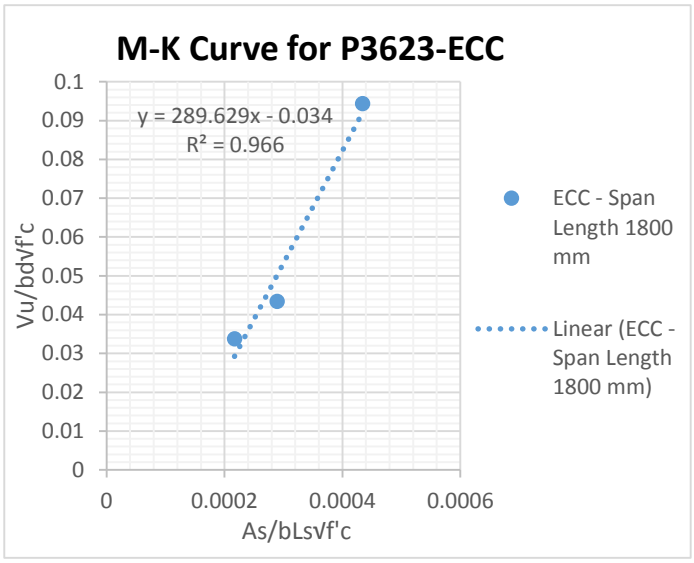

(a)

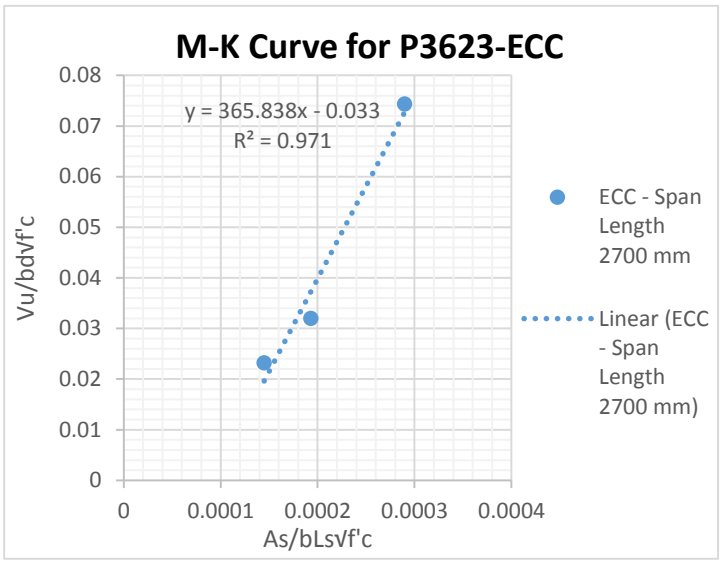

(b)

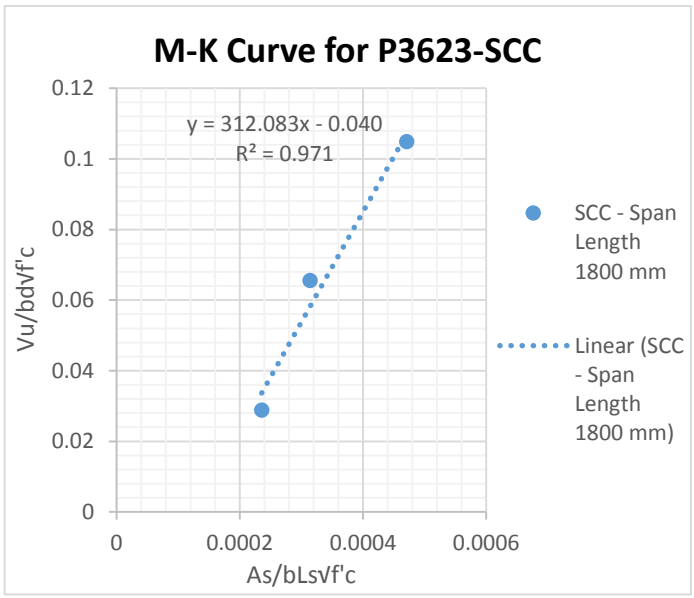

(c)

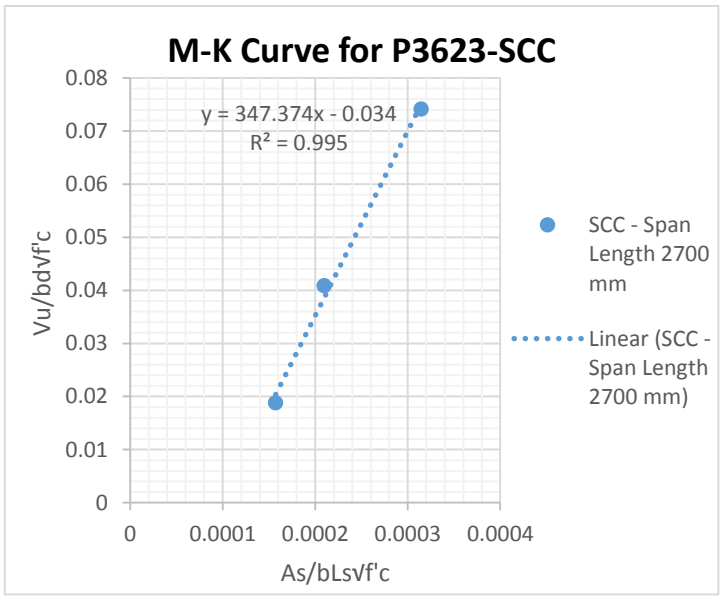

(d)

Figure 6.11: Typical m-k curves for total span of 1800 mm and 2700 mm (a,b) ECC composite slab, (c,d) SCC composite slab

Table 6.11: Accuracy ratio comparison between finite element (FE) results and experimental data

Composite slab	m	k	$\tau_{u,Rd}$ (N/mm^2)	Ratio (Experimental/FEA) m	k	$\tau_{u,Rd}$
			1.295218			1.01024
			0.954635			
P3623-ECC-1800-FE Model	289.63	0.0337	0.78434	1.006	1.0259	1.01174
			1.30848			
			0.96584			1.01297
P3623-ECC-1800-Experimental	291.38	0.0345	0.79452			
			1.39896			0.9337
			1.03198			
P3623-SCC-1800-FE Model	312.08	0.0398	0.84849	0.956	0.8511	0.9258
			1.30627			
			0.9554			0.91923
P3623-SCC-1800-Experimental	298.38	0.0339	0.77996			

Shear bond parameters (m and k) and shear bond capacity of SCC and ECC composite slab are compared in Table 6.11. It is found that FE models and experimental slabs produced close values of m, k and shear bond (ratio experimental to FEA value ranges between 0.91 and 1.01) which shows FE models are reliable in predicting shear bond capacity of both SCC and ECC composite slabs. On the other hand, shear bond capacity of ECC and SCC composite slabs are found to be identical. This can be attributed to the presence of only embossments as shear transfer device in the tested slab. The use of embossments and shear stud connectors together was found to produce higher shear bond resistance of ECC composite slab compared to their SCC counterparts (Hossain et al. 2014).

6.6 Summary and Conclusions

As presented in this chapter, two FE models were developed mainly for SCC and ECC composite slabs. It was found that the FE model using displacement control method was the best model to simulate the experimental composite slab with respect to load-displacement response and also in terms of the computational running time. Results obtained from SCC/ECC finite element models are relatively close to the experimental results in terms of load-deformation response, ultimate load and shear bond prediction.

CHAPTER 7 – SUMMARY, CONCLUSIONS AND RECOMMENDATIONS

7.1 Summary and Conclusions

Two nonlinear finite element (FE) models for ECC and SCC profiled steel-deck composite slabs were developed using ABAQUS/Explicit. Experimental results of ECC and SCC composite slabs are used to develop and verify the performance of two FE models. Load-displacements of experimental slabs tested under four point loading with variable shear spans are primarily used to fine tune the numerical parameters and material properties. Simulating ultimate load capacity with acceptable mid-span displacement, while preventing the early longitudinal shear failure and interface slip was the main aim for developing the FE models for SCC and ECC profiled steel-deck composite slabs. The composite action between the steel and concrete was solely achieved with steel deck embossments. Develop FE models are used to simulate the behavior of numerical ECC/SCC composite slabs having variable total and shear span to evaluate ultimate load/moment resistance and the shear bond characteristics. The following conclusions are drawn from the study:

- Extensive parametric studies suggested that nonlinear finite element models for composite slabs using ABAQUS/Explicit should employ the following:
  - Displacement control analysis with coupling load constraint
  - Element type C3D8R for concrete and S4R for steel deck with mesh element size of 25 mm
  - Modified concrete damage plasticity model to define the compression and tension behaviour of SCC and ECC
  - Surface-to-surface explicit penalty contact interaction between profiled concrete and steel sheet allowing for finite sliding at the interface
  - The tangential behaviour with penalty friction coefficient of 0.5 and normal interface behaviour with hard contact pressure-overclosure
  - Implementing smooth step amplitude for gradual application of loading
- Load-displacement response of obtained from experiment and FE analysis verified superior ductile failure behavior of ECC composite slabs compared to their SCC counterparts. Normally shear strength and ultimate failure load capacity of composite slab decreased with the increase of shear span.

- FE models are found good in simulating load-displacement response, ultimate load/moment capacity and steel deck-concrete shear bond compared to experimental test data. These models can be used reliably to simulate the structural behaviour of composite slabs.
- Design aids presented the form tables for the prediction of load/moment resistance and steel-concrete shear bond of ECC and SCC composite slabs can be used for practical design applications. However, these aids are valid only for P3623 Canam profiled steel deck used in the development of FE models.

7.2 Recommendations for Future Research Studies

The following recommendations are suggested for future research studies:

1) More experimental and numerical ABAQUS FE modeling works should be performed on profiled steel-deck composite slab by using additional interface connections (such as shear studs) in addition to the embossments to generate better steel concrete composite action.
2) The available "concrete damage plasticity" model in ABAQUS/CAE was designed with "concrete softening" behaviour for post-cracking. ECC behaviour is more or less like a ductile metal, ABAQUS concrete model should be modified to suite ECC. ECC should be modeled as steel rather than concrete to account for its post-tensioning performance in future studies.
3) FE models should be developed with more experimental data employing more shear span generating more points to prove more accurate prediction of shear bond parameters (m and k) and hence steel-concrete shear bond capacity.
4) One limitation of the proposed nonlinear ABAQUS FE models is due to their development based on insufficient concrete-steel deck interaction (only embossments). FE models should be developed by using sufficient concrete-steel deck connections (use of embossments and shear studs) simulating better structural behavior of composite slabs that can differentiate shear bond capacity of ECC and SCC composite slabs.

REFERENCES

Abdullah, R. (2004). *Experimental Evaluation and analytical modeling of shear bond in composite slabs* (Doctoral dissertation, Virginia Polytechnic Institute and State University).

Abdullah, R., and Easterling, W. S. (2007). Determination of composite slab strength using a new elemental test method. *Journal of Structural Engineering,* 133(9), 1268-1277.

Afefy, H.M.E.D., and Mahmoud, M. H. (2014). Structural performance of RC slabs provided by pre-cast ECC strips in tension cover zone. *Construction and Building Materials,* 65, 103-113.

ASCE (1984). Specifications for the design and construction of composite slabs, ASCE, NY.

ASTM C39 (2012). Standard method for Compressive Strength of Cylindrical Concrete Specimens. Annual Book of ASTM Standard, ASTM International, West Conshohocken, PA, USA.

ASTM C78 / C78M (2010). Standard Test Method for Flexural Strength of Concrete. Annual Book of ASTM Standard, ASTM International, West Conshohocken, PA, USA.

Bouzoubaâ, N. and Lachemi, M. (2001). Self-compacting concrete incorporating high volumes of class F fly ash: Preliminary results. *Cement and Concrete Research,* 31(3), 413-420.

Canam Group. (2006). *Canam – Steel Deck Catalogue*. Canada: CANAM, pp. 14-17. http://files.canam-construction.com/files/canam-steel-deck-catalogue-canada.pdf (Accessed date: 14-10-2014).

Chen, S. (2003). Load carrying capacity of composite slabs with various end constraints. *Journal of Constructional Steel Research,* 59(3), 385-403.

Chen, S., and Shi, X. (2011). Shear bond mechanism of composite slabs – A universal FE approach. *Journal of Constructional Steel Research,* 67(10), 1475-1484.

CSA-S16 (2009). Limit state design of steel structures. Canadian Standards Association, Etobicoke, Ontario, Canada.

Daniels, B. J., and Crisinel, M. (1993a). Composite slab behaviour and strength analysis. Part I: Calculation procedure. *Journal of Structural Engineering,* 119(1), 16-35.

Daniels, B. J., and Crisinel, M. (1993b). Composite slab behaviour and strength analysis. Part II: Comparisons with test results and parametric analysis. *Journal of Structural Engineering,* 119(1), 36-49.

Dassault Systèmes Simulia Corp. (2013). ABAQUS/CAE Documentation, Version 6.13-3. Providence, RI, USA (www.simulia.com).

Davis, R. O., and Selvadurai, A. P. S. (2002). Plasticity and geo-mechanics. Cambridge University Press, Cambridge.

Ekberg, C. E., and Schuster, R. M. (1968). Floor systems with composite form-reinforced concrete slabs. Final report, IABSE, 8th congress, New York, NY, 385-394.

Eurocode 4 (1994). Design of composite steel and concrete structures, British Standard Institution, London.

Ferror, M., Marimon, F., and Crisinel, M. (2006). Designing cold-formed steel sheets for composite slabs: An experimentally validated FEM approach to slip failure mechanics. *Thin-walled structures,* 44(12), 1261-1271.

Gholamhoseini, A., Gilbert, R. I., Bradford, M. A., and Chang, Z. T. (2014). Longitudinal shear stress and bond-slip relationships in composite concrete slabs. *Engineering Structures,* 69, 37-48.

Hayakawa, M., Matsuoka, Y., and Shindoh, T. (1994). Development and application of superworkable concrete. *In RILEM PROCEEDINGS*, 183-190.

Hossain, K. M. A. (1995). In-plane shear behaviour of composite walling with profiled steel sheeting, PhD Thesis, University of Strathclyde, Glasgow, UK.

Hossain, K. M. A. (2014). Behaviour of ECC link slab for joint-free bridge construction. *Proc. Structural Faults + Repair,* Imperial College, London, UK.

Hossain, K. M. A., Alam, S., Meugoufu, H., Anwar, M. S., and Julkarnine, K. M. (2014). High-performance composite flooring systems with CANAM profiled steel decks. NSERC, Engage Report, Department of Civil/Eng., Ryerson University, 3OP.

Hossain, K. M. A., and N. Vinay, N. (2012). Shear bond resistance of composite slabs with high performance concrete. The 6th International Conference on Advanced Composite Materials in Bridges and Structures, ACMBS-VI, Kingston, Ontario, Canada.

Hossain, K. M. A. and Wright, H. D. (1998). Performance of profiled concrete shear panels. Journal of Structural Engineering, ASCE, 124(4), 368–381.

Hossain, K. M. A. and Wright, H. D. (2004a). Performance of double skin-profiled composite shear walls — experiments and design equations, Can. J. Civ. Eng. 31, 204–217.

Hossain, K. M. A. and Wright, H. D. (2004b). Experimental and theoretical behavior of composite walling under in-plane shear, Journal of Constructional Steel Research 60, 59–83.

Khayat, K. H. (1999). Workability, testing, and performance of self-consolidating concrete. *ACI Materials Journal,* 96(3), 346-353.

King MS-S10 SCC (2014). http://industrial.kpmindustries.com/Product_Catalogue/products/Concrete/MS-S10_Self-Consolidating Concrete.aspx (Accessed date: 10-09-2014).

Lachemi, M., Hossain, K. M. A., Lambros, V. and Bouzoubaa, N. (2003). Development of cost-effective self-compacting concrete incorporating fly ash, slag cement or viscosity modifying admixtures. *ACI Materials Journal*, 100(5), 419-425.

Lam, D. and Qureshi, J. (2008) Prediction of longitudinal shear resistance of composite slabs with profile sheeting to Eurocode 4. In: The Regency Steel Asia International Symposium on innovations in structural steel, RSA-ISISS 2008, 1 December, 2008, Singapore.

Lee, J., and Fenves, G. L. (1998). Plastic-damage model for cyclic loading of concrete structures. *Journal of Engineering Mechanics, ASCE,* 124(8), 892-900.

Li, V. C. (1993). From micromechanics to structural engineering: the design of cementitious composites for civil engineering applications. *Journal of Structural Mechanics and Earthquake Engineering*, 10(2), 37–48.

Li, M., and Li, V. C. (2011). Cracking and healing of engineered cementitious composites under chloride environment. *ACI Materials Journal,* 108(3).

Lublinear, J., Oliver, J., Oller, S., and Onate, E. (1989). A Plastic-Damage Model for Concrete*. International Journal of Solids and Structures*, 25(3), 299-326.

Lubliner, J. (1990). PLASTICITY THEORY (Revised Edition). Berkeley: University of California.

Makelainen, P. and Sun, Y. (1999). The longitudinal shear behavior of a new steel sheeting profile for composite floor slabs, *Journal of Constructional Steel Research*, 49, 117–128.

Marimuthu, V., Seetharaman, S., Arul Jayachandran, Chellappan, A., Bandyopadhyay, T. K. and Dutta, D. (2007). Experimental studies on composite deck slabs to determine the shear-bond characteristic $m-k$ values of the embossed profiled sheet, *Journal of Constructional Steel Research*, 63, 791–803.

Mohammed, B.S. (2010). Structural behavior and $m-k$ value of composite slab utilizing concrete containing crumb rubber, *Construction and Building Materials*, 24 (7), 1214–1221.

Mohammed, B.S., Al-Ganad M.A. and Abdullahi, M. (2011). Analytical & experimental studies on composite slabs utilising palm oil clinker, *Construction and Building Materials*, 25(8) 3550-3560.

Nawy, E.G. (2008). Concrete Construction Engineering Handbook. 2ed Edition, Taylor & Francis Group.

Porter, M. L. and Ekberg, C. E. (1971). Investigation of cold-formed steel-deck reinforced concrete floor slabs. First specialty conference on cold-formed steel structures – University of Missouri-Rolla, 179–85.

Porter, M. L. and Ekberg, C. E. (1976). Design recommendations for steel deck floor slabs. *Journal of Structural Division, ASCE,* 102(11), 2121–36.

Rafiei, S. (2011). Behaviour of double skin profiled composite shear wall system under in-plane monotonic, cyclic and impact loadings. (Order No. NR93387, Ryerson University (Canada)). *ProQuest Dissertations and Theses,* 338.

Rafiei, S., Hossain, K. M. A., Lachemi, M., Behdinan, K., and Anwar, M. S. (2013). Finite element modeling of double skin profiled composite shear wall system under in-plane loadings. *Engineering Structures,* 56(1), 46-57.

Sahmaran, M., Li, M., & Li, V. C. (2007). Transport properties of engineered cementitious composites under chloride exposure*. ACI Materials Journal,* 104(6).

Sahmaran, M., Lachemi, M., Hossain, K.M.A. and Li, V.C. (2009a). Internal curing of engineered cementitious composites for prevention of early age autogenous shrinkage cracking. *Cement and Concrete Research,* Elsevier Ltd., 39(10) 893–901.

Sahmaran, M., Lachemi, M., Hossain, K.M.A., Ranade, R., and Li, V.C. (2009b), "Influence of Aggregate Type and Size on Ductility and Mechanical Properties of Engineered Cementitious Composites," ACI Materials Journal, 106(3), 308–316.

Schuster, R. M. (1976). Composite steel-deck concrete floor systems. *Journal of Structural Division, ASCE,* 102(5), 899–917.

Sherir, M. A. A., Hossain, K.M.A. and Lachemi, M. (2014). Fracture energy characteristics of engineered cementitious composites incorporating different aggregates. *4th International Structural Specialty Conference*, CSCE, Halifax, NS.

Veljkovic, M. (1996). Behaviour and Resistance of Composite Slabs. Phd Thesis, Lulea University of Technology, Lulea, Sweden.

Wright, H. D., Evans, H. R., and Harding, P.W. (1987). The use of profiled steel sheeting in floor construction. *Journal Construction Steel Research,* 7(4), 279–295.

Widjaja, B. R. (1997). "Analysis and Design of Steel Deck-Concrete Composite Slabs," PhD Dissertation, Virginia Polytechnic Institute and State University, Blacksburg.

Zhou, J., Quian, S., Van Breugel, K., and Ye, G. (2010). Engineered cementitious composites with low volume of cementitious materials. *Proceedings FramCos-*, 7(1), 1551-1556.

APPENDICES

A.1 ABAQUS model results for ECC composite slab (Total Span of 1800 mm):

ABAQUS Curve for Shear Span = 300 mm		ABAQUS Curve for Shear Span = 450 mm		ABAQUS Curve for Shear Span = 600 mm	
Displacement at center (mm)	**Total Reaction Force (kN)**	**Displacement at center (mm)**	**Total Reaction Force (kN)**	**Displacement at center (mm)**	**Total Reaction Force (kN)**
0	-.00006	0	-.000001	0	-5.8E-05
3.19E-05	-.00687	0.000563	-.155384	1.92E-05	0.033232
0.000906	-.0999	0.001244	-.158525	0.000173	0.020035
0.001597	.15281	0.000965	.155229	0.000155	0.021018
0.002707	-.20152	0.001399	-.165737	0.000948	-0.00603
0.003132	-.20091	0.002764	.1907	0.002031	-0.06928
0.005253	.24132	0.00541	-.067484	0.003926	0.03907
0.008213	-.32472	0.008666	-.064128	0.006419	-0.0163
0.012898	.21879	0.012248	.274808	0.009388	0.001265
0.016896	.62712	0.016956	-.224424	0.013465	0.276755
0.023663	.94061	0.022837	-.538944	0.018301	0.045737
0.0323	.50828	0.029275	-.040904	0.024293	-0.07082
0.041951	.33626	0.03754	.021579	0.031267	0.173335
0.053176	.95412	0.045616	-.162988	0.039505	0.172767
0.065766	.95469	0.057056	.55525	0.048684	0.272245
0.080872	2.22069	0.06883	.454367	0.059493	-0.07668
0.098562	.83062	0.082271	.657226	0.071398	0.270975
0.116769	2.22239	0.097161	.558878	0.084758	0.280929
0.138053	2.27498	0.113203	1.144694	0.099188	0.218717
0.160305	3.47767	0.131101	1.110878	0.115436	0.616306
0.185496	3.87623	0.15241	1.090205	0.133623	0.798528
0.211666	2.34779	0.174648	1.326821	0.153528	1.026614
0.241667	3.48759	0.199102	1.603656	0.174956	0.766814
0.27332	3.99458	0.224869	1.631155	0.198164	0.934205
0.307967	5.30822	0.253835	1.824648	0.223156	1.353802
0.346174	4.69462	0.285295	2.339837	0.250357	0.903811
0.385755	4.3281	0.316658	2.764723	0.279008	1.355395
0.427776	5.784	0.352446	2.796499	0.309633	1.361323
0.473552	6.07133	0.389096	3.357475	0.342329	1.947898
0.522613	7.42541	0.428267	3.172843	0.377133	2.115293
0.573833	8.47219	0.469711	4.161653	0.413864	2.027669
0.626952	8.45054	0.513461	4.719494	0.45275	2.089445
0.683989	10.61189	0.557183	5.56464	0.493645	2.665666
0.704726	9.67488	0.604491	5.598864	0.536985	2.854042

0.649095	-4.52227	0.655442	6.20112	0.58221	3.367718
0.665029	5.87563	0.70694	6.77304	0.629478	3.288547
0.748987	9.98266	0.761416	7.568544	0.679164	3.749376
0.790178	11.00957	0.819245	7.898208	0.730961	4.015733
0.83917	10.31674	0.877153	8.591952	0.784847	4.147219
0.897118	11.22245	0.878896	12.295872	0.840928	4.772208
0.965957	11.65954	0.920458	4.08719	0.89944	5.496192
1.02166	12.80885	0.971975	7.021872	0.956778	4.893552
1.09079	13.63234	1.03584	6.679488	1.0088	4.504056
1.15998	15.25747	1.1027	7.112784	1.06971	4.59252
1.23042	16.33901	1.16986	7.158912	1.13429	1.290653
1.30436	17.56186	1.23812	7.879632	1.20158	3.723811
1.37869	18.59078	1.30721	8.34072	1.26796	5.042976
1.45446	19.80691	1.37984	8.849904	1.3392	4.396858
1.53374	22.05509	1.4542	9.782208	1.41279	4.235966
1.61566	22.5625	1.5303	10.439136	1.48864	4.071341
1.70313	23.53718	1.6078	11.070864	1.56687	5.077536
1.78938	24.69101	1.68999	11.49312	1.64716	5.234256
1.88068	26.47584	1.7737	12.186912	1.72966	5.192736
1.97195	28.27402	1.8601	12.7992	1.81413	5.74224
2.06639	29.5847	1.94801	13.620864	1.90061	5.964672
2.16335	31.78013	2.03595	14.559312	1.98916	6.433344
2.26289	33.34248	2.12849	14.926224	2.08009	6.889344
2.36317	35.97758	2.22268	15.948	2.17287	7.280304
2.46572	38.02565	2.31898	16.622496	2.26767	7.684656
2.57028	38.49696	2.41648	17.44008	2.36426	7.903872
2.67996	40.23787	2.51526	17.965392	2.46277	8.368704
2.79152	42.40714	2.61671	19.03896	2.56317	8.538096
2.90417	43.70458	2.72099	20.093664	2.66559	9.191232
3.01957	45.60024	2.82665	20.833824	2.76985	9.434688
3.13569	47.88298	2.9351	21.745152	2.87612	9.921312
3.25341	48.16368	3.04391	22.610544	2.9837	10.2624
3.34491	58.21536	3.15563	23.972928	3.09327	10.90867
3.44975	54.26112	3.26887	25.060944	3.20453	11.01538
3.58778	54.86736	3.38347	26.603424	3.31755	11.70619
3.70752	56.86704	3.49912	27.559776	3.4325	12.18331
3.83563	58.59072	3.6172	28.013184	3.54881	12.11309
3.95611	59.07792	3.73691	29.463024	3.66659	12.72686
4.4049	56.40528	3.85898	29.855712	3.78614	12.9445
4.61365	57.17568	3.98087	31.283664	3.90714	13.82866
4.93157	59.87184	4.1049	32.076624	4.02961	13.91774

5.09411	61.1016	4.22922	33.165216	4.15323	14.95843
5.26451	59.22672	4.35654	34.226208	4.27809	15.68405
5.41118	56.7456	4.48406	34.986576	4.40476	16.07986
5.56783	57.624	4.6144	36.297408	4.53229	16.07011
5.72288	57.44928	4.74407	37.615248	4.66085	16.18373
5.86831	59.30016	4.87626	38.74464	4.79033	18.63163
6.01475	59.98752	5.00506	39.12648	4.92142	17.72688
6.15886	62.24688	5.13666	40.237488	5.05306	19.6272
6.30285	61.97328	5.27049	39.05136	5.18589	19.40592
6.44725	63.5184	5.40624	40.429248	5.31959	19.31419
6.58833	66.97056	5.54176	41.290704	5.45422	19.35096
6.74598	68.43072	5.67657	42.189792	5.58959	19.70621
6.89543	68.49216	5.8135	42.856608	5.72532	21.36274
7.04233	71.9328	5.95203	42.96456	5.86137	23.49374
7.1888	69.16896	6.08944	45.152064	5.99825	24.89074
7.33527	70.30992	6.22693	44.668416	6.13656	26.08699
7.49049	74.05152	6.3676	45.168336	6.27516	26.13749
7.64197	72.87504	6.50639	44.974176	6.41446	27.20122
7.79274	72.50784	6.64646	40.692624	6.55433	27.40637
7.94895	76.78224	6.7835	42.180864	6.69412	27.56117
8.10437	76.32768	6.9249	42.75552	6.83421	27.39254
8.2602	73.34736	7.0651	42.810672	6.97451	28.27642
8.41519	78.39312	7.20591	44.276784	7.11481	28.43011
8.57026	81.2688	7.34763	42.488016	7.25572	28.8263
8.72638	81.22128	7.48893	43.058976	7.39649	28.75248
8.8857	77.83392	7.6298	43.256592	7.53702	29.31413
9.05089	79.48944	7.77385	44.62296	7.6794	29.88379
9.21377	78.88176	7.91492	43.6128	7.82168	30.30946
9.3802	80.72688	8.05665	42.414096	7.9637	30.42413
9.54431	77.17872	8.19734	44.2932	8.1057	30.93965
9.70642	79.97664	8.338	43.108416	8.24754	32.04134
9.86847	78.94848	8.47684	44.764896	8.38865	31.37232
10.0329	80.45232	8.61979	44.055456	8.5301	32.18237
10.1881	81.00336	8.75913	44.57568	8.67073	32.67403
10.3467	80.07456	8.8989	43.072176	8.8108	33.72374
10.5025	80.34768	9.03808	45.843888	8.95041	34.40914
10.6529	80.61792	9.17774	46.695072	9.08916	33.51379
10.8076	86.48928	9.31683	45.540672	9.22765	34.80581
10.9691	85.7688	9.45409	45.170736	9.36493	30.19589
11.1172	80.43312	9.58877	44.565648	9.50234	29.87669
11.2699	81.62544	9.72661	43.188672	9.63859	29.69952

11.4069	85.41936	9.86158	45.138192	9.77457	30.68352
11.542	90.32832	9.99711	46.3656	9.90952	30.42149
11.6776	98.36736	10.1312	47.883696	10.0361	31.84224
11.8178	97.7136	10.263	45.464688	10.1702	31.89355
11.9552	100.47456	10.3941	47.994288	10.3019	33.35074
12.0908	98.29728	10.5252	48.03744	10.4329	33.00686
12.2303	97.81008	10.6535	47.673984	10.5624	32.95262
12.3631	104.38224	10.7798	49.42224	10.6913	33.02621
12.4899	102.5952	10.9087	47.204544	10.8187	34.44869
12.6271	99.42432	11.0336	51.34896	10.9447	34.36646
12.7582	101.98464	11.1573	47.825328	11.0694	34.85611
12.8827	103.54416	11.2801	50.7648	11.1924	35.97072
13.0165	102.94848	11.4018	48.45264	11.3137	35.54501
13.152	107.78544	11.5206	49.20576	11.4335	36.84086
13.2785	105.9024	11.6367	48.98016	11.5511	36.04186
13.406	108.09792	11.7531	46.588176	11.6681	36.8088
13.5479	106.03776	11.8684	48.05088	11.7832	37.28275
13.6711	114.37728	11.9791	44.214144	11.8965	36.73272
13.7898	107.62128	12.0901	44.214	12.0086	36.47246
13.9096	110.39232	12.2026	46.303824	12.119	36.14778
14.0218	105.46464	12.3119	47.34888	12.228	36.63315
14.1293	109.80336	12.4172	46.686	12.3351	37.48141
14.238	110.59872	12.5218	46.541424	12.4395	37.97595
14.3484	110.70048	12.6259	46.697712	12.5429	38.42347
14.455	105.72	12.7258	47.412	12.6448	38.54198
14.5558	106.43184	12.8263	47.692128	12.7447	38.60827
14.6534	106.26096	12.9244	46.218768	12.8422	39.11198
14.736	109.73232	13.0202	51.08448	12.9379	38.79682
14.822	104.93232	13.115	48.39792	13.0315	38.23563
14.9138	112.5024	13.2053	45.296784	13.123	38.98582
15.0047	108.39696	13.2962	46.638192	13.2124	38.17765
15.0937	109.06368	13.3841	44.085264	13.2998	38.52542
15.1827	113.12304	13.4704	45.34224	13.3846	38.48261
15.2692	106.6128	13.5553	45.672912	13.4647	37.96738
15.3553	107.23728	13.6369	46.847904	13.5452	37.71173
15.4388	106.9776	13.714	46.86816	13.6242	35.52864
15.5181	96.22992	13.7911	46.48224	13.7	36.3005
15.5993	103.59888	13.8657	48.81456	13.7743	38.2397
15.6824	101.75808	13.9388	48.33408	13.8471	38.22187
15.7606	100.58736	14.0101	45.957072	13.9169	38.7248
15.8343	104.56368	14.0779	49.06176	13.9848	38.01026

15.9047	110.71056	14.1423	48.38112	14.0507	38.28078
15.9713	95.71632	14.2052	45.311328	14.1133	38.10587
16.0365	104.79072	14.2665	47.192208	14.1736	38.28914
16.0982	108.20448	14.3258	50.99328	14.2332	38.77192
16.1586	97.39296	14.3844	48.2304	14.2901	38.53376
16.2174	103.57056	14.4384	50.29152	14.3446	38.38478
16.2736	97.32672	14.4919	48.32256	14.3984	38.32248
16.3202	99.264	14.5419	46.56816	14.4487	39.29386
16.3649	104.27376	14.5903	48.49872	14.4961	38.1588
16.4148	97.9992	14.6366	44.712096	14.5429	38.22955
16.4575	93.15024	14.6812	45.461904	14.5875	38.00427
16.4967	97.28208	14.7233	48.76416	14.6296	38.98912
16.5294	101.76384	14.7642	48.32976	14.6697	39.97051
16.5674	105.54192	14.8005	47.273904	14.7082	38.69394
16.6004	104.2992	14.8368	44.91432	14.7434	38.82478
16.6327	113.6688	14.87	47.8224	14.7775	39.80971
16.6668	102.2784	14.9029	48.1728	14.8095	39.14002
16.6964	101.71008	14.933	45.244752	14.8392	39.15077
16.7238	104.03712	14.9609	48.35664	14.8674	38.60562
16.7486	110.87088	14.9868	46.878384	14.8933	38.0039
16.7705	103.48128	15.0107	44.28576	14.918	38.34886
16.7934	98.61936	15.0331	46.610592	14.9398	38.13317
16.8101	111.08832	15.0546	46.253568	14.9609	38.64938
16.832	108.44784	15.0735	48.05712	14.9797	38.32462
16.8467	103.19904	15.0917	48.828	14.9969	38.65147
16.8604	103.64496	15.1079	48.8784	15.0134	39.4823
16.8742	104.99664	15.1224	46.790496	15.028	39.22326
16.8861	103.11744	15.1354	47.189904	15.0415	39.16963
16.8988	107.40048	15.1461	47.662176	15.0525	33.8929
16.9105	110.62032	15.1561	45.466992	15.0629	34.3117
16.9196	109.68816	15.1656	43.833744	15.0721	38.29795
16.9264	106.03488	15.1725	45.956496	15.0793	38.57707
16.9345	104.77248	15.1791	44.196816	15.0867	37.21834
16.9359	102.17712	15.1851	48.94752	15.0916	39.7332
16.9405	102.36816	15.1896	44.496528	15.0974	36.29304
16.9432	107.12016	15.1922	45.524112	15.1007	39.13147
16.9457	112.73568	15.1961	46.486608	15.1035	37.05917
16.9458	111.46416	15.1982	46.49928	15.1055	35.18525
16.947	110.29728	15.1991	46.812192	15.1073	37.89984
16.9471	114.00144	15.2002	45.931008	15.1077	34.53845
16.945	105.5016	15.202	44.664864	15.1096	38.82698

16.9466	105.56352	15.2019	44.99592	15.1094	38.11522
16.9475	110.4384	15.2019	45.838896	15.11	37.74302
16.9465	106.40256	15.2025	42.83352	15.1102	34.87301

A.2 ABAQUS model results for SCC composite slab (Total Span of 1800 mm):

ABAQUS Curve for Shear Span = 300 mm		**ABAQUS Curve for Shear Span = 450 mm**		**ABAQUS Curve for Shear Span = 600 mm**	
Displacement at center (mm)	**Total Reaction Force (kN)**	**Displacement at center (mm)**	**Total Reaction Force (kN)**	**Displacement at center (mm)**	**Total Reaction Force (kN)**
0	0.020733	0	.	0	0.020502
1.3E-05	0.028074	-0.00068	-.07761	-0.00011	-0.04148
-0.00017	0.127533	-0.00095	-.02681	0.000105	-0.11659
-0.00024	0.429996	-0.00085	-.34552	0.000331	0.007826
-0.00015	0.2434	0.000538	-.02623	0.000296	0.085318
0.000189	0.47443	0.00096	-.11218	0.00049	-0.02901
0.002894	0.937402	0.000803	-.33307	0.000903	0.265219
0.002852	1.020811	0.001779	-.10551	0.001566	0.077564
0.005369	0.75191	0.00204	.04069	0.002267	0.065889
0.007893	1.308125	0.004053	-.09832	0.002957	0.139847
0.009666	1.76004	0.005677	-.06584	0.00378	0.09089
0.01217	1.777541	0.007165	.0259	0.004921	0.156761
0.015159	2.304413	0.008582	.35371	0.006233	0.273515
0.019828	2.363443	0.012288	.8886	0.007599	0.345349
0.023746	2.392978	0.015954	.54224	0.009587	0.293499
0.029273	3.202483	0.018646	1.11509	0.011457	0.297626
0.035893	2.800992	0.023821	.97523	0.013824	0.271641
0.042115	3.086203	0.028904	1.07074	0.016776	0.449674
0.050235	3.219125	0.034678	1.76524	0.019885	0.466973
0.059138	3.807062	0.041001	1.93391	0.023103	0.810946
0.067879	4.33705	0.048606	1.94576	0.02696	0.913147
0.078136	4.850112	0.056035	2.08974	0.031059	1.075752
0.089095	5.453616	0.063621	2.34739	0.035449	1.127717
0.101145	6.237792	0.072959	2.66712	0.03986	1.258008
0.113501	6.656064	0.082676	2.69419	0.044921	1.562251
0.127363	7.29336	0.091596	2.95051	0.049971	1.504123
0.141113	8.415168	0.102757	3.05765	0.055849	1.83444
0.157274	9.148848	0.114267	4.09141	0.062126	2.015352
0.174046	10.12205	0.127993	4.1312	0.068849	2.206939

0.192091	10.38538	0.140402	4.88088	0.075932	2.439168
0.211251	11.78798	0.153741	5.20037	0.083371	2.499202
0.231203	12.20794	0.169633	5.86699	0.091228	2.78941
0.252847	13.32427	0.184658	6.52488	0.099597	3.232454
0.274893	14.17186	0.200434	7.07966	0.107784	3.452674
0.298009	15.30955	0.216979	7.62878	0.117204	3.635328
0.321686	16.72157	0.236028	8.27275	0.126788	4.218797
0.347627	18.01195	0.25412	9.66744	0.136735	4.409318
0.371997	19.75493	0.274298	9.89698	0.147169	4.527634
0.397151	22.0464	0.293853	10.86475	0.158201	5.02152
0.42281	24.14904	0.314916	12.13642	0.169566	5.340576
0.449503	27.02942	0.337352	12.55277	0.181414	5.615328
0.478629	29.09645	0.359214	13.07179	0.193756	6.091392
0.750355	16.75853	0.38404	13.99392	0.206352	6.5352
0.732624	16.42733	0.408543	15.3119	0.219374	6.953664
0.792962	12.7873	0.432903	16.10717	0.233065	7.256064
0.838295	16.94347	0.45976	17.03194	0.247053	7.611744
0.84797	19.08456	0.485866	18.87106	0.261216	8.08128
0.886394	16.91467	0.514448	18.78941	0.276267	8.710128
0.928592	18.97488	0.541638	20.76859	0.291664	8.683152
0.961889	19.63258	0.571666	22.12411	0.307151	9.663264
0.997009	20.24362	0.601792	23.89267	0.323191	10.15978
1.03258	21.14194	0.632567	24.7811	0.339581	10.51421
1.07148	22.04126	0.665091	25.95802	0.356848	11.30462
1.10827	22.86739	0.698758	26.96102	0.374524	11.83315
1.1467	24.17798	0.732402	28.02605	0.392249	12.60331
1.18552	24.72394	0.766427	30.12811	0.410972	13.11374
1.22687	25.67914	0.80115	31.63589	0.429744	13.70952
1.26707	26.89272	0.767103	22.14398	0.448729	14.20814
1.30858	28.19597	0.802994	11.2392	0.468413	14.9401
1.35169	29.13864	0.827207	10.44389	0.488295	15.77342
1.39395	30.33547	0.864948	13.07453	0.50892	16.28813
1.43595	31.00205	0.901094	14.89666	0.529657	16.98547
1.477	32.44325	0.935307	15.40066	0.908912	17.3779
1.52235	33.70776	0.972381	15.56554	0.915439	4.701197
1.56818	34.63877	1.00888	16.35706	0.943242	7.40808
1.61215	34.76635	1.046	16.96286	0.96747	7.651392
1.65793	35.52302	1.08396	17.46211	0.99383	9.403392
1.7043	36.53765	1.12247	18.26794	1.01967	10.25366
1.75137	36.81614	1.162	18.60888	1.0452	11.75395
1.79985	38.28014	1.20086	18.99288	1.07124	12.06946

1.84849	40.73458	1.24164	19.66406	1.09804	12.36998
1.89526	40.89187	1.2829	20.31653	1.12516	12.73675
1.94229	43.55256	1.32456	20.87395	1.1515	12.63485
1.98721	44.71195	1.36685	21.62578	1.17885	13.18498
2.0354	44.07907	1.40942	22.14984	1.20653	13.21128
2.08604	45.68429	1.45217	22.67419	1.23387	13.31232
2.13542	46.42565	1.49634	23.1347	1.26145	13.45747
2.18714	49.09344	1.54038	23.84347	1.28925	13.99786
2.23895	49.5024	1.58515	24.43997	1.31723	14.2655
2.29215	52.32384	1.63003	25.20422	1.34573	14.68666
2.34231	52.18416	1.67557	25.82779	1.37361	14.70086
2.39425	54.66768	1.72169	26.71555	1.40208	15.1152
2.44503	55.38624	1.7683	27.26549	1.43024	15.5245
2.49456	56.0856	1.81434	27.81341	1.45866	15.76426
2.54773	57.7296	1.86035	28.66296	1.487	16.14245
2.59959	59.49312	1.90715	29.18794	1.51505	16.45862
2.65315	61.05168	1.95378	29.99232	1.54394	16.69786
2.70574	62.77776	2.00035	30.73512	1.57244	17.1193
2.75634	62.70144	2.04813	31.32178	1.60111	17.30568
2.80916	64.48848	2.0964	32.00894	1.62963	17.50056
2.86132	64.5984	2.1445	32.62469	1.65834	17.87414
2.91419	67.6992	2.19347	33.02438	1.68665	18.23179
2.96848	68.70048	2.24087	33.9371	1.71511	18.57221
3.01951	69.67104	2.2896	34.87646	1.74344	18.75178
3.07033	70.74144	2.33878	35.57333	1.77172	19.05811
3.22587	71.90976	2.38898	36.35525	1.8	19.36186
3.53113	71.4736	2.43867	36.86842	1.82803	19.6715
3.53204	72.15216	2.48789	37.74034	1.85583	19.87666
3.64523	72.58112	2.53792	38.06064	1.88371	20.28422
3.6939	73.19104	2.58747	39.18514	1.91135	20.70346
3.78816	73.3152	2.63755	39.38803	1.93896	20.84813
3.84695	75.1728	2.68627	40.65734	1.96611	21.21302
3.92091	76.23552	2.73703	40.78234	1.99339	21.32851
3.98831	78.53808	2.78831	41.62243	2.0204	21.81874
4.05387	80.71248	2.8391	42.50846	2.04713	22.07083
4.11772	81.88752	2.88949	43.21934	2.0736	22.35245
4.18059	83.98368	2.93971	43.87085	2.09983	22.56797
4.23605	85.0992	2.98796	44.45285	2.1259	22.74917
4.2919	83.74656	3.0384	45.45418	2.15184	23.22014
4.35024	86.59344	3.08887	45.79608	2.17742	23.5199
4.40773	86.75664	3.13873	46.83744	2.20271	23.79979

4.46385	87.204	3.18823	47.15304	2.22798	24.0756
4.5181	89.11584	3.23719	48.08352	2.25279	24.25555
4.57473	90.43776	3.28655	48.74496	2.27744	24.59856
4.62929	92.23344	3.33525	49.62096	2.30163	24.79214
4.68369	91.58448	3.51254	49.75008	2.32568	25.13251
4.73631	93.81552	3.57227	47.33501	2.34921	25.30147
4.78733	93.69168	3.6214	50.49264	2.3726	25.38341
4.82674	91.17264	3.68442	50.12448	2.39563	25.88117
4.87768	91.24176	3.74451	51.04608	2.41837	26.20066
4.92517	92.34096	3.82282	50.66448	2.44061	26.50685
4.9734	93.57744	3.88279	51.58224	2.46241	26.80277
5.01846	92.16096	3.94644	52.24464	2.48399	27.02496
5.05878	95.15376	4.00294	53.35344	2.50513	27.15427
5.10872	97.0464	4.05583	53.92464	2.52598	27.23606
5.15473	97.44288	4.1075	54.55536	2.54632	27.41222
5.19192	97.8048	4.15832	55.00944	2.56632	27.72173
5.23577	100.1645	4.20741	56.11056	2.5869	27.96946
5.27783	99.20688	4.25657	56.8752	2.60643	28.51949
5.31792	101.1451	4.31986	57.35616	2.62582	28.89115
5.35649	101.6654	4.36067	56.85264	2.64441	28.77374
5.39637	102.5678	4.40593	57.46704	2.66257	28.99598
5.43302	103.7477	4.45058	58.54224	2.68051	29.30102
5.47117	102.6019	4.49574	58.63248	2.69766	29.53886
5.50489	102.6451	4.54128	58.98192	2.71447	29.49029
5.53973	104.4874	4.58566	59.67456	2.73094	29.75026
5.57522	104.7821	4.62975	59.61984	2.74684	29.71354
5.60867	104.0424	4.67277	60.21216	2.76241	30.08059
5.64245	103.9848	4.71512	60.468	2.77755	30.24134
5.68635	106.0685	4.75632	61.24128	2.79208	30.58162
5.7165	106.1779	4.79678	61.1112	2.8064	30.49776
5.74657	108.4858	4.83591	61.96656	2.8203	30.53208
5.77663	106.7875	4.87558	62.38512	2.83365	31.10746
5.8056	106.6507	4.91422	62.6568	2.84667	31.28458
5.83246	107.3035	4.95131	62.66832	2.85902	31.1939
5.8576	106.2317	4.98716	62.92368	2.87107	31.26864
5.88294	109.4683	5.02298	63.32064	2.88265	31.30416
5.90826	109.5504	5.05696	64.05744	2.89378	31.85731
5.93314	109.0493	5.0914	64.03584	2.90437	31.55851
5.95387	110.7202	5.12487	64.25808	2.91468	31.92994
5.97735	111.9221	5.15759	64.71936	2.92447	32.02142
5.99998	110.1706	5.18904	65.03136	2.93378	32.47867

6.019	108.2909	5.22019	65.556	2.94273	32.29286
6.03819	110.3808	5.24968	65.6856	2.95113	32.23536
6.05689	108.301	5.27953	66.06432	2.95927	32.3604
6.0718	111.2208	5.3079	66.07008	2.967	32.63333
6.08907	111.3802	5.33528	66.53232	2.97413	32.6677
6.10542	110.9702	5.36176	66.93408	2.98073	32.51798
6.12044	111.9562	5.38741	67.04352	2.98716	32.90285
6.13474	111.8146	5.41186	67.6296	2.99325	32.76864
6.14941	112.3646	5.43532	67.57536	2.99884	32.80651
6.16218	111.731	5.45775	67.9824	3.00411	32.79365
6.17451	111.323	5.48017	68.12928	3.00903	32.87458
6.18548	111.5784	5.50081	68.43552	3.01361	32.5573
6.1955	113.0011	5.52091	68.55456	3.01797	33.02232
6.20549	110.4878	5.54014	68.79936	3.0217	33.46325
6.21518	111.371	5.55856	69.096	3.02522	32.994
6.22379	112.0042	5.57623	69.27504	3.0285	33.23683
6.23159	111.9566	5.593	69.52176	3.03136	33.37766
6.23791	112.0642	5.60873	69.5496	3.03404	33.40224
6.24376	112.813	5.62357	69.8136	3.03657	33.26832
6.24948	112.3262	5.63791	70.01904	3.03858	33.22128
6.25514	113.0458	5.65134	70.01568	3.04032	33.16694
6.26267	112.524	5.66413	70.272	3.04192	33.13075
6.26713	111.0835	5.67592	70.32432	3.04332	32.97965
6.26977	111.2573	5.68499	69.8856	3.04452	33.17026
6.27296	112.5475	5.6957	70.5264	3.04556	33.31018
6.27275	111.8395	5.70552	70.35792	3.04625	33.23491
6.276	112.8298	5.71424	70.31664	3.04695	33.22416
6.27784	113.2224	5.72229	70.65456	3.04736	33.20851
6.28013	112.2859	5.72961	70.98336	3.04765	33.18422
6.28144	110.4797	5.73714	71.0136	3.04786	33.19046
6.28318	110.0808	5.74308	70.58928	3.0477	33.3215
6.28416	113.9578	5.74922	70.94688	3.04786	33.25397
6.28465	111.4104	5.75483	70.91136	3.0478	33.22392
6.28454	111.3288	5.75941	70.7664	3.04787	33.43363
6.28604	111.8314	5.76356	71.18928		
6.2839	111.3701	5.76721	71.08944		
6.2853	112.3742	5.77042	71.40864		
6.28393	111.4512	5.77308	70.98144		
		5.77492	70.92192		
		5.77656	70.90032		
		5.77806	71.07456		

		5.77898	70.84704		
		5.78003	70.96752		
		5.78075	71.6232		
		5.78082	71.3136		
		5.78138	71.39472		
		5.78129	71.25504		
		5.78128	71.13408		
		5.78128	71.3424		